Enhanced Digital Imager Defect Analysis with Smaller Pixel Sizes

by

Rahul Thomas

B.A.Sc., Simon Fraser University, 2013

Thesis Submitted in Partial Fulfillment of the
Requirements for the Degree of
Master of Applied Science

in the
School of Engineering Science
Faculty of Applied Sciences

SIMON FRASER UNIVERSITY

Summer 2016

Approval

Name: Rahul Thomas

Degree: Master of Applied Science

Title: Enhanced Digital Imager Defect Analysis with Smaller Pixel Sizes

Examining Committee:

Chair: Dr. Ash M. Parameswaran, PEng
Professor

Dr. Glenn Chapman, PEng
Senior Supervisor
Professor

Dr. Marinko Sarunic, PEng
Supervisor
Associate Professor

Dr. Israel Koren
External Examiner
Professor
Department of Computer and Electrical Engineering
University of Massachusetts at Amherst

Date Defended/Approved: August 3rd, 2016

Abstract

Digital imager pixels are shrinking resulting in an increased rate of pixel defects. These defects are known as “Hot Pixels” that are permanent in nature and develop in-field. The number of hot pixels in a given digital imager increases over time.

This research experimentally measures defect rates for pixels from 7 µm to those in the cellphone camera range, as low as 1µm. New software algorithms and techniques have been developed to compensate for increasing noise levels in the 2 to 1 µm range. This has allowed the creation of an empirical model that provides accurate projections of defect rates as pixel size decreases and sensitivity increases. Results show that the hot pixel rate increases by 8.9 times as pixels shrink by a factor of 2. Additionally, digital imagers allow us to explore soft errors (known as single event upsets) in a way that can’t be done in traditional ICs.

Keywords: CMOS; imager defects; reliability; hot pixels; SEUs; growth rate

Acknowledgements

I would like to thank my thesis committee members Glenn, Israel, Marinko and Ash for participating in my thesis defence and research. Specifically, I want to extend my gratitude to my senior supervisor Dr. Glenn Chapman for giving me this opportunity to work on this research project while working fulltime in the ASIC design industry. Your inspiration, patience, and guidance through this project are much appreciated. I would also like to thank Dr. Israel and Zahava Koren for their continual insight and advice throughout my research.

A special thanks to all my colleagues at SFU and PMC-Sierra for your participation and assistance along the way. Additionally, I want to thank my management at Microsemi (PMC-Sierra) for enabling me to undergo a Masters degree during my employment.

Lastly, I want to thank my parents, siblings and friends for your endless support and prayers throughout my studies. Above all, I would like to take this opportunity to thank God for being my strength and guide throughout my education.

Table of Contents

Approval ii
Abstract iii
Acknowledgements iv
Table of Contents v
List of Tables vii
List of Figures viii
List of Acronyms xi
Glossary xii

Chapter 1. Introduction 1
1.1. Digital Photography Overview 1
1.2. Market Trends 2
1.3. Defects in Digital Imagers 6
1.4. Summary 9

Chapter 2. Image Sensors and Hot Pixel Defects 10
2.1. Overview 10
2.2. Photodetector 10
2.3. Photodiodes 13
2.4. CMOS Sensors 14
2.5. Sensor Comparison 18
2.6. Digital Photography Basics 19
2.6.1. Pixels and Bayer Pattern 20
2.6.2. Image File Formats 21
2.6.3. ISO 23
2.6.4. Standard Pixel Response 24
2.6.5. Exposure Time 26
2.7. Permanent Defective Pixel Overview 27
2.7.1. Defective Pixel Response 27
2.7.2. Stuck Defective Pixels 28
2.7.3. Standard Hot Pixels 29
2.8. Hot Pixel Detection 31
2.8.1. Dark Frame Techniques 31
2.8.2. Image Capture Techniques 32
2.9. Summary 33

Chapter 3. Hot Pixel Experimental Results and Analysis 34
3.1. Overview 34
3.2. Hot Pixel Software Detection Algorithms 35
3.2.1. Experimental Process 35
3.2.2. Hot Pixel Detection 37
3.3. Curve Fitting Methodology 43

3.4. Hot Pixel Defect Growth Model 46
3.4.1. Hot Pixel Defect Growth with Pixel Size 47
3.4.2. Power Law 47
3.4.3. Hot Pixel Growth Analysis Combining Pixel Size and ISO 49
3.5. Industry Trends to Lower Pixel Sizes 51
3.6. Cellphone Imager Defect Analysis 53
3.6.1. Enhanced Dark Frame Calibration Methods 53
3.6.2. Growth Model for Cellphone Imagers 55
3.7. Summary 61

Chapter 4. Single Event Upsets in Digital Imagers 62
4.1. Overview 62
4.2. SEU Defects in Digital Imagers 63
4.3. SEU Defect Detection Methods 65
4.3.1. Experimental Overview 65
4.3.2. System Noise Consideration 69
4.4. SEU Defect Classification 70
4.5. Summary 73

Chapter 5. Single Event Upsets Experimental Results and Analysis 74
5.1. Overview 74
5.2. Experimental Results 74
5.3. SEU Analysis 76
5.4. SEU Charge Analysis 85
5.5. Summary 86

Chapter 6. Conclusion 88
6.1. Overview 88
6.2. Future Research 90
6.3. Concluding Thoughts 92

References 93
Appendix A. List of APS Imagers 98

List of Tables

Table 2.1. Typical Absorption values in Silicon (data taken from [18]).....12

Table 3.1. Power Law Fitted Constants with Error Bounds.....49

Table 3.2. Sensor Area for Camera Numbers Tested 53

Table 3.3. Updated Power Law Fitted Constants with Error Bounds 56

Table 4.1. Averaged Baseline Noise Values 70

Table 5.1. SEU Defect Rates for 3 APS Digital Imagers (t=10s, ISO 1600).....84

List of Figures

Figure 1.1 Growth Profile for various Camera types in Canada (after [1]).....3

Figure 1.2 Cellphone Shipments from 2007-2014 (after [2]).....4

Figure 1.3 Cellphone Megapixel Counts from 2004-2010 (after [3]).....5

Figure 1.4 Cellphone Megapixel Counts from 2004-2010 [7].....7

Figure 2.1. Semiconductor Energy Bands at 0ºK 11

Figure 2.2. Photoelectric process.....12

Figure 2.3. P-N Junction Diode I-V Curve (taken from [19]) 13

Figure 2.4. Photodiode Circuit Behavioural model.....14

Figure 2.5. 3T CMOS Pixel Design 16

Figure 2.6. 4T CMOS Pixel Design 17

Figure 2.7. 3T CMOS Pixel Layout (taken from [22]).....18

Figure 2.8. CMOS vs. CCD imager shipments 19

Figure 2.9. Red, Green and Blue color filters 20

Figure 2.10. Bayer Pattern Demonstration 21

Figure 2.11. Image Processing Pipeline.....22

Figure 2.12. Ideal Pixel Response 24

Figure 2.13. ISO effects on pixel response.....25

Figure 2.14. Examples of (a) Underexposed and (b) Overexposed Images 26

Figure 2.15. Example Hot Pixel Defect.....28

Figure 2.16. Comparing the dark response of imager pixels: (a) good pixel, (b) standard hot pixel, (c) hot pixel with offset [29].....29

Figure 2.17. Hot Pixel Intensity Increase with Exposure Time.....32

Figure 3.1. Hot Pixel Experimental Process Overview.....36

Figure 3.2. Examples of two detected hot pixels 38

Figure 3.3. Fitted Intensity Curve of a True Hot Pixel (y = 1.9011x + 0.1349, R^2 = 0.9434) 39

Figure 3.4. Fitted Intensity Curve of a False Hot Pixel (y = 0.3918x + 0.1866, R^2 = 0.0831) 39

Figure 3.5. Overall Defect Identification Flow 41

Figure 3.6. Example Residual Plot 44

Figure 3.7. Residual Plot Example – Ideal 45

Figure 3.8. Residual Plot Example - Problematic 45

Figure 3.9. Residual Plot Example - Low Error 46

Figure 3.10. Residual Plot Example - High Error 46

Figure 3.11. APS Defect rate/year/mm^2 vs pixel size for fixed ISO (taken from [32]) 47

Figure 3.12. Fitted power law for APS defect density (D=defects/year/mm2) vs. pixel size S (µm) and ISO (I) [34] 50

Figure 3.13. Camera count as a function of pixel size and ISO – (a) Prior: 2006-2012 (b) Current: 2016 51

Figure 3.14. Expanded data Fitted power law for APS defect density (D=defects/year/mm2) vs. pixel size S (µm) and ISO (I) 57

Figure 3.15. Expanded data Fitted power law for APS in the 1 to 2.5 µm pixel range: defect density (D=defects/year/mm2) vs. pixel size S (µm) and ISO (I) 57

Figure 3.16. Residuals of fitted power law for APS defect density; Residual Log(D) (D=defects/year/mm^2) vs. pixel size S (µm) and ISO 58

Figure 3.17. Residuals of fitted power law for APS defect density; Residual Log(D) (D=defects/year/mm^2) vs. pixel size S (µm) 59

Figure 3.18. Residuals of fitted power law for APS defect density; Residual Log(D) (D=defects/year/mm^2) vs. ISO) 60

Figure 4.1. Examples of SEUs 63

Figure 4.2. SEU Detection Algorithm demonstrating an SEU that was detected in image ‘j’ and not present in images ‘j-1’ and ‘j+1’ 68

Figure 4.3. SEU types – simple SEU spot (bottom), SEU streak (top left) and SEU cluster (top right) 71

Figure 4.4. Experimental SEU Streak 1 72

Figure 4.5. Experimental SEU Streak 2 72

Figure 5.1. Simple Experimental SEU Streak (snapshot of 5x6 pixels – 31.3µm x 37.6 µm) 75

Figure 5.2. Complex SEU Streak (snapshot of 12x17 pixels in size – 75.12µm x 106.42µm) 76

Figure 5.3. Distribution of SEUs per image (ISO 6400, t=30s) – Canon 5D MII, 6.26 µm – Peak ~ 3 events/image 77

Figure 5.4. Distribution of SEUs per image (ISO 6400, t=10s) – Canon 5D MII, 6.26 µm – Peak ~ 2 events/image 77

Figure 5.5. Distribution of SEUs per image (ISO 6400, t=3.2s) – Canon 5D MII, 6.26 µm – Peak ~ 1 event/image 78

Figure 5.6. Distribution of SEUs per image (ISO 6400, t=1s) – Canon 5D MII, 6.26 µm – Peak ~ <1 event/image 78

Figure 5.7. Distribution of SEUs per image (ISO 1600, t=30s) – Canon 5D MII, 6.26 µm – Peak ~ 1 event/image 79

Figure 5.8. Distribution of # of SEUs per image (ISO 1600, t=10s) – Canon 5D MII, 6.26 µm – Peak ~ 1 event/image 79

Figure 5.9. Distribution of # of SEUs per image (ISO 1600, t=3.2s) – Canon 5D MII, 6.26 µm – Peak ~ < 1 event/image 80

Figure 5.10. Distribution of # of SEUs per image (ISO 1600, t=1s) – Canon 5D MII, 6.26 µm – Peak ~ 1 event/image 80

Figure 5.11. Average number of SEUs per image vs exposure time for 1600 and 6400 ISO settings (log scale) 82

Figure 5.12. Average number of SEUs per image vs ISO (for a 30s exposure) for 2 cameras scaled to camera A (36x24mm) 83

Figure 5.13. Normalized SEU rate λ(c) as a function of the charge 86

List of Acronyms

3T	Three Transistor
4T	Four Transistor
APS	Active Pixel Sensor
BER	Bit Error Rate
CCD	Charge-Coupled Device
CFA	Color Filter Array
CMOS	Complementary Metal-oxide Semiconductor
DLSR	Digital Single-lens Reflex
GUI	Graphical User Interface
GPU	Graphics Processing Unit
HDR	High Dynamic Range
IC	Integrated Circuit
ISO	International Organization for Standardization
LCD	Liquid Crystal Display
OS	Operating System
SEU	Single Event Upset
SFU	Simon Fraser University
SRAM	Static Random Access Memory

Glossary

Dark Frame Calibration	An experimental process in which multiple images are taken with a pitch dark background for a given imager. ISO and exposure times are swept to collect all combinations. The resulting images are analyzed using specialized software to detect hot pixel defects.

Chapter 1.

Introduction

1.1. Digital Photography Overview

Since its inception in the commercial camera world in about 1999, digital imager technology has dominated the world of photography and is becoming ubiquitous, spreading into everyday products from cell phones to cars via embedded sensors. A digital imager's advantage over traditional film based models is vast. It gives the user freedom to explore creative photography. Additionally, the cost of owning a digital camera is lower than film over the entire lifespan of the camera itself. Photographic sensitivity (ISO) is also increased and can be manipulated from shot to shot in digital photography. Digital imagers enable users to instantly review images before they are printed and provide the opportunity to make improvements and adjustments with software tools. The applications for digital imagers are quite wide spread. Firstly in the photographic industry, implementations range from compact digital cameras and cellphone cameras for the average photographer to full DSLRs for professional use with customizable ISO, exposure and shooting settings. Other applications include industrial manufacturing, security cameras and use in the medical field. In scientific applications, specialized high speed cameras are used for characterization of events that occur very quickly. Enhancing the physical camera itself, image processing software tools such as Photoshop have made it easier to edit and manipulate digital images thus increasing the overall ease of photography. A standard digital imager consists of a pixel sensor, processing electronics and software, and memory for image storage. The pixel sensor is

the heart and soul of every digital imager and its design, study and reliability will be the focus of this thesis.

In addition to hardware advancements in imagers, innovation in the software industry has greatly pushed imaging capabilities. Most modern imagers have software and processing algorithms that are inbuilt into the imager's functionality. For example, in traditional film based photography the concept of white balance was purely set by the type of film used and controlled via the process itself. In digital imagers, white balance is a software enhanced feature that can be automatically adjusted or varied in DSLR imagers. With Digital RAW files (the digital equivalent of photographic negative) white balance can be adjusted after shooting unlike film. Thus the power of the digital camera is the combination of hardware and software functionality. Unlike film based cameras, the image that is delivered to the user is greatly processed with software in digital cameras. This creates complications that arise when assessing the quality and defect behaviour of digital imagers. Our research looks into such issues and discusses solutions for imager defect analysis.

1.2. Market Trends

Given the popularity and increasing demand for digitalized imagers, one could expect the growth of such systems to have increased dramatically in comparison to its predecessor, film based cameras. Figure 1.1 displays the sales profile for different camera types; specifically comparing film based manufacturing sales to digital camera sales.

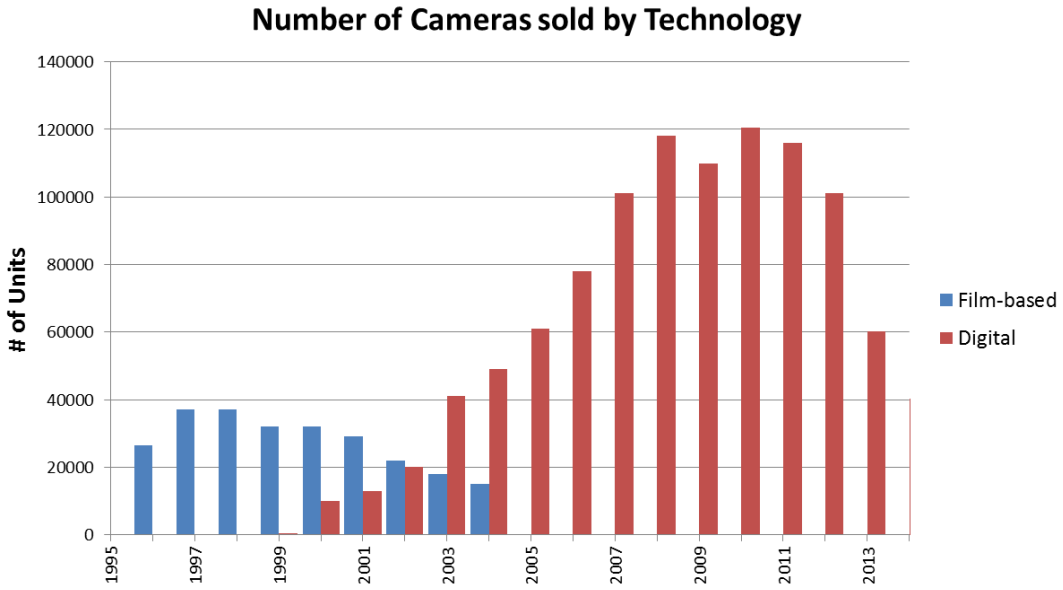

Figure 1.1 Growth Profile for various Camera types in Canada (after [1])

It's not surprising that as the chart moves into the early 2000's, digital imagers begin to rapidly take over the market by 2005 making legacy analog cameras almost non-existent from a market point-of-view. Another interesting point is that the DSLR market started out quite small but has increased in popularity as time progressed indicating a greater interest in the field in today's modern society.

The main trend that one should observe is towards the end of the chart. As we get close to 2013 and onwards to present day, the number of digital cameras in general that are being manufactured is decreasing. The main reason is due to the effectiveness and wide-spread availability of cellphone cameras. Figure 1.2 displays the growth of the cellphone industry over a period of 8 years.

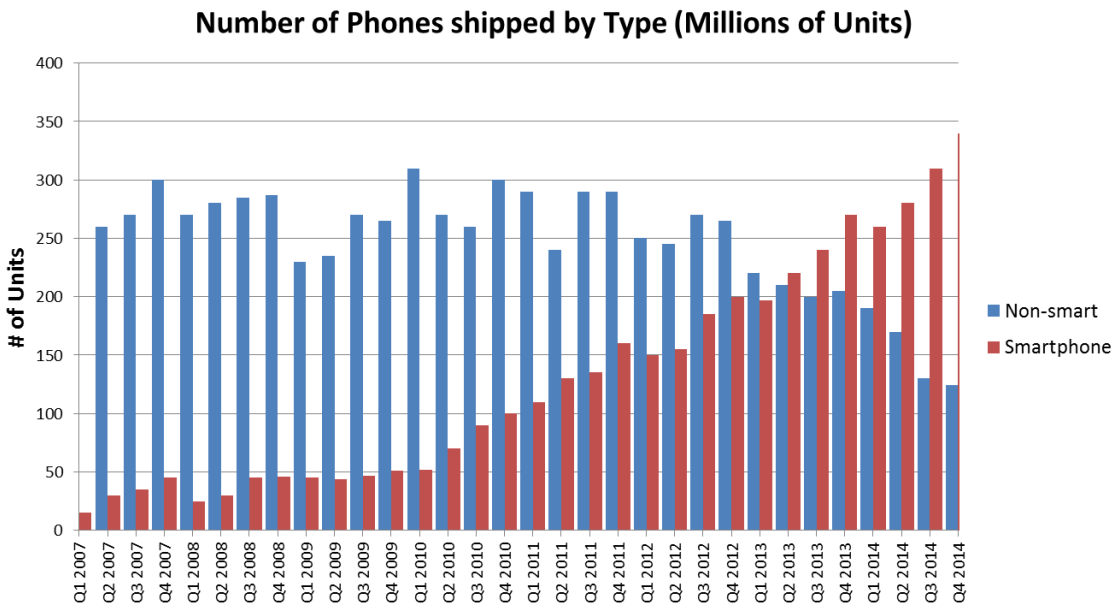

Figure 1.2 Cellphone Shipments from 2007-2014 (after [2])

The biggest trend from the above figure is that the mobile market is converting to smartphones. The main factor for this change is that many of the features that are available in mainstream digital cameras can now be found in typical smartphones. Firstly increasing mega-pixel counts in recent cellphone generations have been an effective marketing technique especially in the younger demographic. Additionally, modern Android OS systems are now providing users with the ability to capture images in their RAW format with ISO, exposure time and other shooting controls. Apple iOS based cellphones are rumoured to have such functionality in the near future (circa 2016). The overall picture here is that people are switching to cellphone cameras as their primary snapshot camera which greatly impacts the current trend in which manufacturers are heading with respect to next generation imagers. Figure 1.3 shows a plot of cellphone megapixel counts as percentage of sales from 2004 – 2010. It is clear the cellphone imagers contain much of the standard features that modern digital imagers possess. Current day cellphones can have pixel counts greater than 20 megapixels. As pixel counts increase, the general trend is to decrease the pixel size itself. The result is a reduction in overall pixel quality and sensitivity. The main goal of manufacturers is to design for increased density with quality and sensitivity being secondary focuses leading to inherent trade-offs with this design approach.

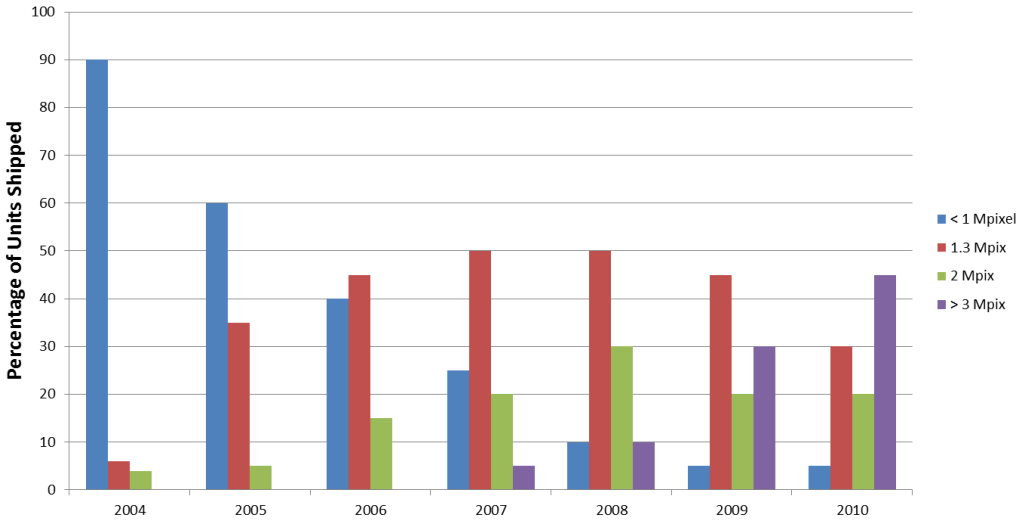

Figure 1.3 Cellphone Megapixel Counts from 2004-2010 (after [3])

Given the market dynamics outlined above, cellphone manufacturers are looking at ways to improve camera performance while reducing costs. As mentioned earlier some of these marketing techniques involve advanced software and control features in the camera applications. However, the main push in the industry is to enhance sensor design in order to increase overall pixel count in the sensor of the imager. A sensor, put simply, is an array of multiple pixels where each pixel holds the value of charge of the incident light. The inherent result of increased cellphone camera usage is a drive to enhance these sensors via a decrease in pixel size and an increase in the sensitivity of the imager itself. Traditional digital photography is accustomed to sensors with pixels in the 5-10 µm range. Even the latest cutting-edge DSLR sensors contain pixels in the 3-5 µm range. However, in the cellphone image sensor realm these pixel sizes are much smaller. Most mainline cellphone imagers contain pixels in the 2-4 µm range. As manufacturers look for more efficiency in their processes, these pixels sizes are getting shrunk to as low as 1 µm and potentially even smaller sizes. There are trade-offs in pixel sensitivity, noise immunity and image quality for smaller pixel sizes. Higher megapixel counts are easy to sell even at lower image performance. One important concern in the reliability segment is whether or not pushing pixel sizes to sub-micron levels has an effect on the overall reliability and defect growth behaviour of the sensor. Note that all pixels in this thesis are assumed to be square.

1.3. Defects in Digital Imagers

The science of reliability engineering and defect analysis is rather vast and is an entire topic of its own. Simply put, the term reliability can be thought of as the probability of long term success. As it applies to manufacturing, reliability is the inherent ability of a product to function properly over its expected lifetime. Reliability benchmarks differ from product to product depending on use-case, price points and expected life time and use of the product itself. In digital imagers, reliability is a very important discussion as their lifecycle is fairly long and certain imagers are used for high precision captures. These make an understanding of imager defects vital and necessary in the design and manufacturing of digital imager sensors. Manufacturers typically don't focus on long term defects as they entertain the idea of consumers purchasing updated models over time. However, if the defect rates are at a level such that defects are noticeable in a short time frame, it makes this area of research very relevant to sensor designers, especially cellphone camera manufacturers.

The cause of defects is one that has been greatly debated in literature. Two classes of defects exist; manufacturing time defects and infield developed defects. Defects that occur at manufacturing time are a cause of fabrication camera defects. These defects occur at time zero in a camera's lifetime. Material degradation on the other hand creates defects that are caused due to inherent decay and alteration in semiconductor structure layers such as thin films and gate oxides [4, 5]. These defects show an inherent clustering behaviour in defect manifestation. These defects are caused by an internal source. For example, if there was an inconsistency with the process that causes defects down the line in the imager's lifetime, these defects would be seen in a particular area of the sensor in clusters as that particular region degrades.

Infield defects on the other hand are caused by external random sources that damage pixel cells creating faults which occur over the imager's lifetime. These defects are random in nature. Past research [6] has shown that the major causes of defects in imagers are external random sources that occur in field rather than material degradation. One reason for this is that unlike mainstream ICs, digital sensors are not constantly used

but rather used only for brief periods of time when taking photos. This in turn limits the use and exposure of the digital imager IC itself. Modern ICs such as microprocessors are used quite extensively and are generally stressed in their operational modes which in turn lead to a greater chance of material degradation.

Defects in imagers, though not always obvious and known to the average photographer, are evident and increase as time progresses. Photography is unique unlike traditional ICs in that defects can be identified in both location and intensity. These defects can be classified into two classes. The first class of defects are known as permanent or hard defects which are formed infield. It is important to note that these defects are created or formed during the lifetime of the imager and not at fabrication (i.e. formed infield). The other class of defects are known as temporary or soft defects which are temporal and cause a defective behaviour that is not permanent. Regardless of the class of defect, defects in imagers occur at the pixel level and are detected in the output image that is created as a result of capturing the input light intensity of a scene. A defect causes the original response of a particular pixel to be degraded such that it causes detectable errors in the output of pixel (i.e. visible in the image itself). Figure 1.4 displays the most common permanent defect types.

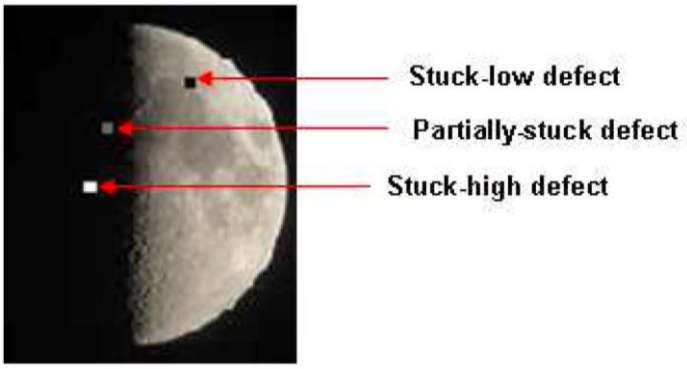

Figure 1.4 Cellphone Megapixel Counts from 2004-2010 [7]

Permanent defective pixels are pixels that constantly exhibit defective behaviour regardless of the environment or time. Several types of defects have been classified in previous research [8] and been reported in various digital sensor and photography

forums and discussions. Overall, these pixel defects are classified into two types; stuck pixels and hot pixels. Stuck defects are pixels that are stuck at a fixed value regardless of the incident light intensity – they are either fully saturated (stuck high) or fully dark (stuck low). Additionally, pixels can also be partially stuck in that they are stuck at an intensity value between fully dark and fully saturated. Stuck defects are usually created during fabrication and can be corrected via defect mapping at manufacturing. Previous work [8] has shown that true stuck pixels do not develop over time.

Another permanent defect of most concern is the hot pixel. Hot pixels are pixel defects where the defect intensity is controlled by the pixel's exposure time. Hot pixels also develop at manufacturing but have been found to increase over time unlike stuck pixels [9]. Additionally, hot pixel responses change as the light intensity is increased unlike stuck pixels that have fixed pixel defective responses. This inherent nature of hot pixels make it more difficult to detect, model and even correct. Studies have shown that cosmic rays hitting the image sensor are the likely cause of hot pixels and their growth [10,11]. Past research has focused on identification of hot pixel types, detection algorithms, effects of ISO and exposure rate on hot pixel response and initial creation of a hot pixel growth model [12, 13, 14]. However at the time, the sensors that were analyzed contained larger pixel sizes in the 6-10 µm range. Additionally, these studies mainly focused on DSLR imagers which in turn paved the way for initial hot pixel defect research. This thesis will focus on research at smaller technology nodes (i.e. < 2 µm). As mentioned earlier, current day technology has enabled manufacturers to push pixel sizes down in size, close to the sub-micron level. Advanced DSLR imagers have already begun to enter this range while cellphone imagers are well in the small pixel range. The complication and concerns that arise from these manufacturing trends center around the effects of pixel size on the defect rate. Pixel sensor designers and manufacturers are unaware of the implications of current trends with relation to defect behaviour. In the later chapters, this concept will be explored in detail for various pixel sizes showing the accelerated hot pixel defect growth at lower pixel sizes.

Soft defects, or defects that are temporal, are quite different in nature. Just like other integrated circuits, imagers are all susceptible to transient defects which are seen in-field but are short-lived. These defects are known as Single Event Upsets (SEUs).

SEUs are caused by cosmic radiation particles the strike the imager at random times and locations causing defective pixel locations that are only evident in a single image. SEU defects should be thought of as a temporary injection of charge acting like real exposure to light. Much study has been given to SEUs in digital ICs [15, 16] over the past few years especially as large IC manufacturers are pushing designs to use smaller technology nodes. Literature suggests SEU defects occur 100 times more than permanent defects making them more prominent. However, the behaviour of SEUs and their rate as it applies to digital image sensors has not been discussed. The effects of ISO and exposure time on the SEU growth rate are important to understand as these mechanisms are not present in standard digital ICs and their effects are unknown in literature. Therefore, the understanding of image sensor behavior in the presence of SEUs is vital and will be explored in this thesis.

1.4. Summary

It is evident that digital imagers have become a central part of today's society. The demand for smartphone devices with advanced photography tools has increased leading to manufacturers pushing pixel sizes down to the sub-micron level. This thesis will look at effects of small pixel size on defects, hot pixel behaviour, and SEU behaviour, as it pertains to digital imagers. The remainder of this thesis is organized as follows: Chapter 2 provides a background on digital imager sensors, camera operation and hot pixel theory. Chapter 3 examines the experimental method for detecting hot pixels and provides in-depth analysis for hot pixel behaviour at smaller pixel sizes. Chapter 4 introduces the concept of SEUs and their application in digital imagers. Chapter 5 discusses experimental SEU measurements, detection algorithms and analysis. Lastly, final thoughts, conclusions and recommendations for future research are provided in Chapter 6.

Chapter 2.

Image Sensors and Hot Pixel Defects

2.1. Overview

The sensor is the heart-and-soul of any digital imager system. Its main role is to capture the incoming light intensity based on various settings programmed by the user at data collection. An understanding of sensor design and behaviour in modern commercially-available imagers is vital to assess the behaviour and impact of defects. This chapter will explain the basic behind photo detection and different sensor types. The various parameters and configuration controls available in modern digital cameras such as ISO and exposure rate will be discussed. Additionally, the theoretical behaviour of defects, particularly of hot pixels, will be introduced as they pertain to modern imagers.

2.2. Photodetector

The process of converting incident light energy into electrical energy which can then be digitized by signal processing circuitry is the fundamental function of any photodetector. Light is created by the transition between quantized energy states which in turn creates waves packets known as photons. The energy of a photon is given by Equation 2.1:

$$E = hv = \frac{hc}{\lambda} \tag{2.1}$$

where, h is Planck's constant and v is the frequency of the photon. In order for the incident photon to generate electrical energy within a semiconductor, its photon energy must be greater than the semiconductor's band gap, E_g. In solid state physics, the band gap is defined as a region in the crystal's energy diagram where no electron states exist. The band gap is the energy difference between the semiconductor valence band and the bottom of the conduction band [17]. The different bands are shown in Figure 2.1 below.

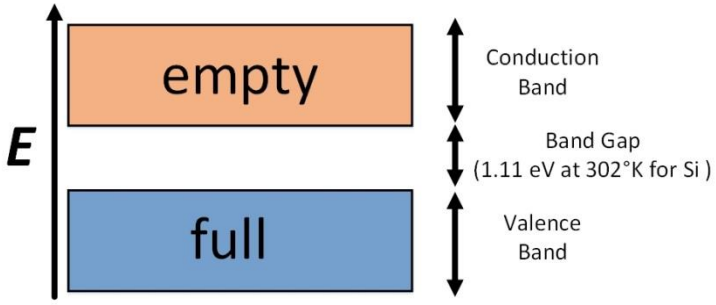

Figure 2.1. Semiconductor Energy Bands at 0ºK

If this condition is satisfied, an electron will be excited from the valence band to the conduction band, creating carriers for electrical energy. A depiction of this process is shown in Figure 2.2. Photons that have energy values less than the band gap energy will not be absorbed by the semiconductor material. Thus for a given semiconductor, there is a cut-off frequency at which all photons below the cut-off will not be absorbed by the semiconductor. This cut-off frequency value is specific to different semiconductor materials. The band gap is the major determining factor of a material's electrical conductivity. Materials with larger band gaps are insulators, while smaller band gaps are generally conductors. In practice, as temperature increases, the thermal energy causes certain electrons from the valence band to be promoted to the conduction band resulting in a flow of charge.

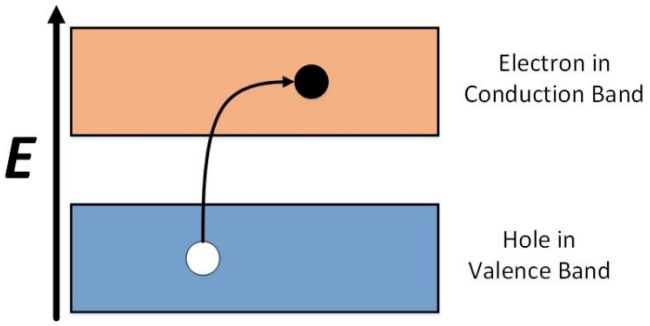

Figure 2.2. Photoelectric process

When a photon penetrates through a semiconductor surface, its initial power I_o, decreases due to absorption within the material. The statistical relationship of the power at a given distance x below the surface of a semiconductor material with an absorption coefficient α (cm^{-1}), is given by the Beer-Lambert Law:

$$I(x) = I_o e^{-x\alpha} \tag{2.2}$$

The absorption behaviour will vary based on the semiconductor type and initial photon energy. Table 2.1 displays the absorption values for the three main components of visible light (Red, Blue and Green) for a silicon type semiconductor. The absorption length is defined as the distance λ into a material where the probability has dropped to 1/e that a particle has not been absorbed.

Table 2.1. Typical Absorption values in Silicon (data taken from [18])

Light Color	Wavelength	Absorption coefficient α (cm^{-1})	Absorption length α^{-1} (μm)
Red	600	3.75×10^3	2.67
Green	525	7.07×10^3	1.41
Blue	450	1.98×10^4	0.51

The complication with the above process is the fact that the actual creation of photo carriers is very transient and does not persist long enough to be measured effectively due to carrier recombination. More advanced techniques are used to prevent recombination and efficiently measure the photoelectric output. Some devices that use these techniques are photodiodes and photogates.

2.3. Photodiodes

The first photodetector that will be discussed is a photodiode. Photodiodes are devices that convert incoming light into electrical energy. A P-N junction diode is a device that is made of a crystal semiconductor. Silicon is the most commonly used semiconductor material for diodes with germanium and gallium arsenide also being used. Impurities are added to the base semiconductor material to create a region that contains negatively charge carriers (electrons) known as n-type and a region that contains positively charged carriers (holes) known as p-type. When these regions are abutted, a transient flow of electrons from the n-type to the p-type occurs and holes from p-type to n-type. This creates a third narrow diffusion region known as the depletion region between the N and P regions where no charge carriers are present. This process is known as the junction effect. The diffusion creates an electric field in the depletion region. This electric field separates charges and creates a net charge effect. A sufficiently higher potential on the P in contrast to the N will cause a flow of electrons from the N to the P through the depletion region. The depletion region does not permit the flow of electrons in the opposite direction. The current-voltage (I-V) characteristics of a typical diode are shown in Figure 2.3.

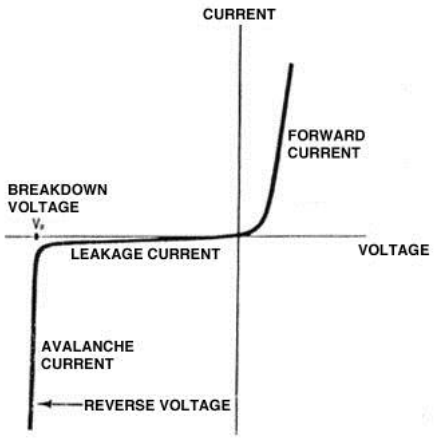

Figure 2.3. P-N Junction Diode I-V Curve (taken from [19])

In essence, a photodiode is a P-N junction diode that is reverse-biased. When an incoming photon has sufficient energy, it will create an electron-hole pair – i.e. the

creation of photo carriers mentioned earlier. With this design, a small amount of current is also produced when no incident light is present. This is current is known as the dark current. Current that is generated through the thermal process in a diode is known as the photoelectric current. Figure 2.4 displays a behavioural model of a photodiode. Note that this is not a physical representation of an actual photodiode, but rather a circuit model that depicts its operation in terms of current and resistance characteristics.

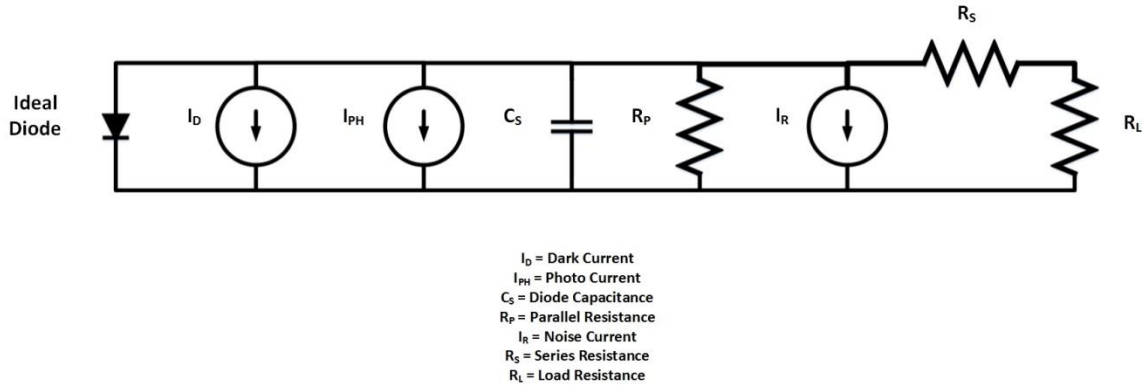

Figure 2.4. Photodiode Circuit Behavioural model

The main advantage of photodiodes is that they can easily be packaged into an array to create a larger photo sensor. Unlike modern CMOS designs that will be discussed later, a photodiode array can be used in high speed applications as it enables parallel readout electronics for quicker image processing. However, the greatest downfall of photodiodes is the large amount of dark current that can be produced. Two main types of sensors exist in digital camera technology; the traditional CCD sensor and the modern CMOS sensor.

2.4. CMOS Sensors

Before exploring CMOS sensors, it should be noted that CCD imagers were the industry favorites in the early stages (early to mid-2000s) of the digital photography boom. At the time, CCD sensors were the most cost-effective option for compact flash and DSLR cameras in the commercial camera market. CCD design and manufacturing

is a very specialized process. However, as CMOS technology progressed, manufacturers moved to using CMOS sensor designs creating a shift in the traditionally accepted sensor market. Today, CMOS sensors completely dominate the digital sensor world and the use of CCDs sensors has been limited to specialized scientific and research applications. Due to these current market trends, this thesis will not focus on CCD sensors, photogates and their defect rates, but rather, will explore the modern-day CMOS sensor.

The CMOS sensor, or more commonly known as the active-pixel sensor (APS), is the most common choice for digital imagers in modern day photography. As indicated in the name, this type of sensor makes use of the Complementary Metal–Oxide–Semiconductor (CMOS) technology process to design a pixel cell. The fundamentals behind CMOS technology is founded on the existence of a complimentary pair of MOS transistors used to create logic functions in digital ICs. This compatibility allows APS sensor to be integrated with other circuits on the sensor.

A large advantage of CMOS technology over other processes is that fact that CMOS designs use much less power. The inherent nature of the design hinges upon the fact that one of the transistors in the pair is always ‘off.’ This in turn reduces power consumption and even gives CMOS circuits higher noise immunity. The only significant power draw is when there is a switch in the logic output. Given these advantages over other semiconductor processes, the CMOS imager is the number one choice for today’s camera manufacturers.

A CMOS pixel is a design that makes use of multiple CMOS transistors to create the pixel cell. Figure 2.5 displays a typical 3 transistor (3T) CMOS pixel design.

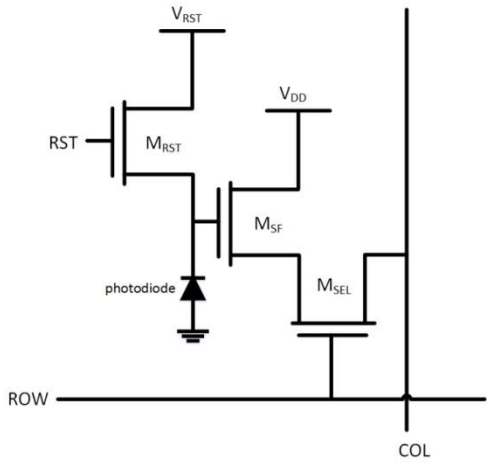

Figure 2.5. 3T CMOS Pixel Design

In the 3T pixel sensor, a photodiode is used to sense the incident light and convert the photon energy to electric energy. An important detail here is that diode is reset to high such that the incident light discharges the diode. In essence, the inversion of the charge is measured at the output of the cell. This eliminates any sub-threshold uncertainties if the measurement was done from low to high. A reset transistor is present to bring the circuit in and out of reset. This functionality is normally used at device power ON where the circuit will be held in reset until software initialization is complete, after which the reset will be lowered to enable operation of the pixel cell (note the active high reset in the diagram). A source follower amplifier is used to collect the output of the photodiode without actually removing the accumulated charge off the diode; essentially acting as a buffering stage. Lastly, a selection transistor enables higher level circuitry to selectively read-out pixel values using row and column selection signals. Although it may not be clear in circuit schematics, in CMOS pixels the photodiode takes up the largest die space in comparison to the rest of the transistors. In modern designs a more complex 4T pixel cell is used [20]. Figure 2.6 displays a typical 4T CMOD design [21]. This is essentially the 3T design with the addition of a transfer transistor just after the photodiode. The transfer transistor adds additional accuracy in extracting the accumulated charge of the photodiode and reduces lag in the pixel circuit. As digital technology has increased over time, more complex designs are being used to increase the dynamic range of the pixel cell in order to provide more functionality and density in

today's digital imagers. Some pixel designs have transistor components that are specifically designed for high-dynamic-range (HDR) captures.

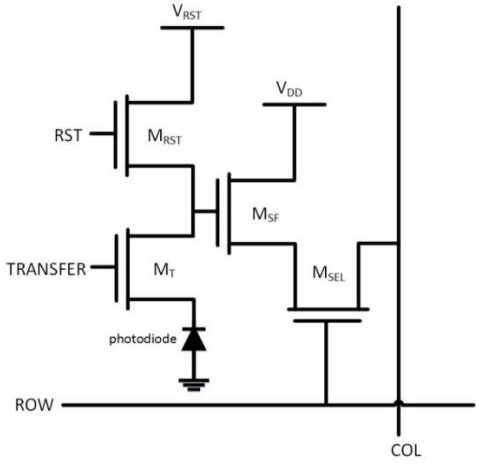

Figure 2.6. 4T CMOS Pixel Design

Pixels are typically put together into a two-dimensional array known as the image sensor. Each pixel is connected to a row and column select line as well as a common reset signal. As mentioned earlier, higher level processing and circuitry can read out pixel values by using the correct row and column signal selection; essentially a large multiplexing feature based on the row and column selections. Modern designs tend to combine the read out values and use circuitry that read out entire rows or columns at a time to increase performance.

Another important concept in pixel design is the fill factor of a pixel. The majority of the pixel area is occupied by the photodetector in order to maximize its exposure to the incident light. However, due to other transistors and control lines in the pixel the entire pixel cannot be used for light detection as some of the area is lost for the other transistor circuitry. This ratio between the areas used for light detection to the total area of the pixel cell itself is known as the fill factor a pixel. Adding more transistors to pixel essentially reduces the fill factor of the pixel increasing the trade-offs between complex designs and overall pixel detector exposure. Figure 2.7 displays the schematic layout of a standard 3T CMOS pixel cell (8 µm pixel size). The fill factor is 49.9% where the photo sensitive area is 4.44µmx6.75µm. As mentioned earlier, in pixel cells, the photodiode

occupies the largest area in comparison to the other transistors. In typical pixel designs the fill factor is around 25%. Micro-lenses are used to increase the light collection efficiency of such designs.

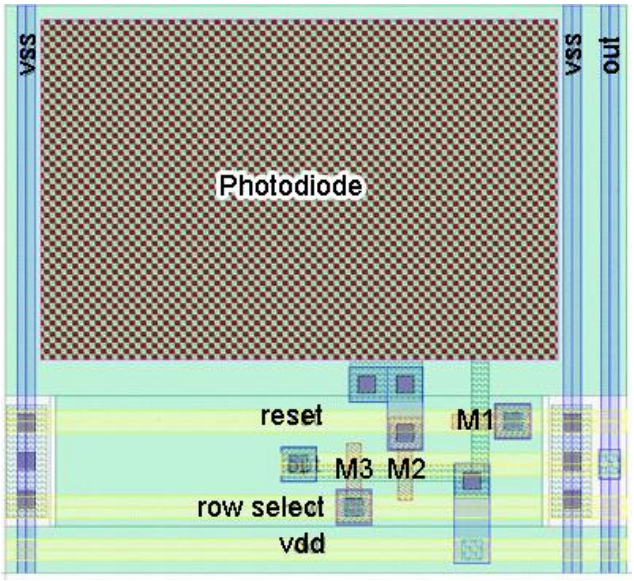

Figure 2.7. 3T CMOS Pixel Layout (taken from [22])

2.5. Sensor Comparison

The main advantage of the CMOS pixel sensor over the CCD is that it is lower cost and easier to manufacture given the widespread availability of CMOS technology and foundries. Given these lower costs, CMOS sensors are the normal choice for high volume and consumer imager applications. CCD sensors however have a larger advantage in low-light applications making them more suitable for scientific and astronomical imaging applications.

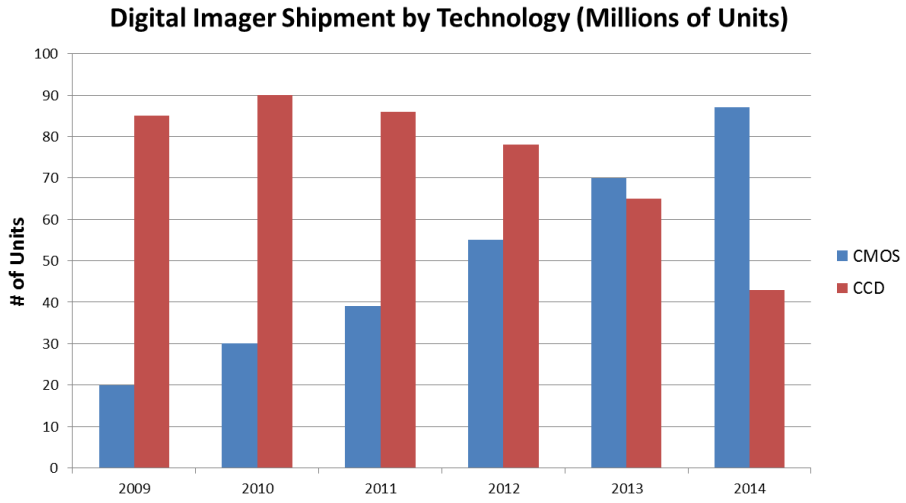

Figure 2.8. CMOS vs. CCD imager shipments

Figure 2.8 display a comparison of CMOS imager vs CCD imager shipment numbers from 2009 – 2014 [23]. Clearly, CCD imagers were the industry leaders earlier the digital photography industry. However as CMOS imager designs became more mature and scalable, CMOS sensors have quickly taken over the market. Today, most consumer digital cameras contain CMOS sensors while CCD sensors are used for more application specific scientific imagers. Given these industry trends and the lower demand for CCD sensors, the remainder of this thesis will focus on CMOS imagers and their defects.

2.6. Digital Photography Basics

As mentioned earlier, an array of physical pixel cells form a digital imager sensor. This sensor is used to collect the incident light for a set amount of time which in turn forms the image. There are many factors that play a role in the image formation including the ISO (sensitivity) and exposure settings as well as the image format and color interpolation methods. These will all be looked at in the next few sections. Here we will take a closer look at digital pixels from a sensor level and how they play a role in capturing the image.

2.6.1. Pixels and Bayer Pattern

APS pixels respond to a wide wavelength range. Thus in a sensor, each photosensitive pixel area is deposited with a colored filter to only allow certain wavelengths of light to be detected by the pixel area. This in turn blocks out other colors only allowing a certain grade of color to pass – Red: 625-740nm, Green: 500-565nm, Blue: 440-485nm. A pictorial depiction of this process is shown in Figure 2.9. As seen from the figure, on a location that has a red filter for example; incident blue light will not transmit light to the photodiode resulting in no accumulated charge at the output of the pixel. Only incident light that contains frequencies in the red spectral range (or that are accepted by the red filter) will be transmitted.

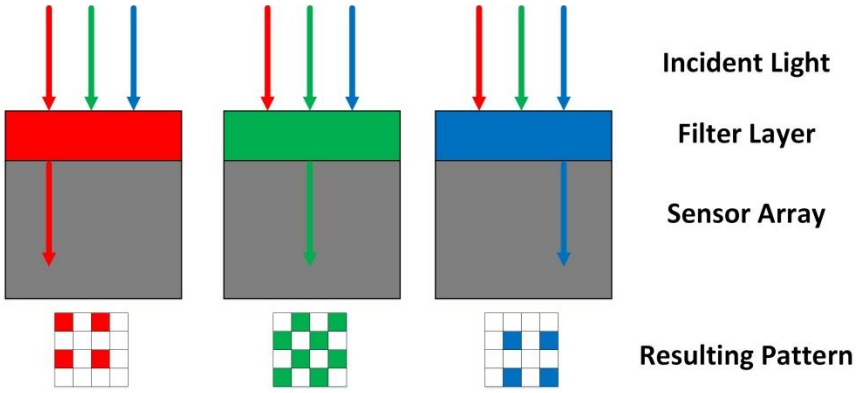

Figure 2.9. Red, Green and Blue color filters

These pixel filters are patterned on a 2x2 square pixel basis. These 2x2 (or 4 pixels in total) filters are known as the Bayer pattern of the imager (i.e. the CFA or Color Filter Array of the Imager). There are several different combinations that are possible but the most common configurations of the Bayer pattern will have two green components, 1 red and 1 blue. The most common configuration is the RGGB Bayer pattern. RGBG and GRGB filters are also possible. A demonstration of this process is shown in Figure 2.10. Bayer patterns typically contain a 2:1 ratio between green to red and blue pixels. This is because the green wavelength is the peak of the emission band and the human eye is most sensitive to the color green.

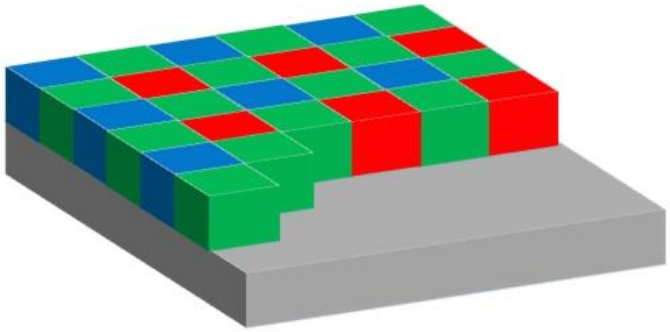

Figure 2.10. Bayer Pattern Demonstration

Using the above technique, the sensor will output a collection of charge values based on a pixel's particular Bayer color and the incident light. Together these are collected together to form the image which uses a pixel value range to depict the light intensity at that location. Essentially the output image is a series of pixel values based on the main RGB color scheme. Though this process is not intuitive, the advantages of this are seen during image compression and interpolation techniques. Image formats and their pixel ranges will be explained in the following sections. A particular imager's CFA pattern will be embedded in the meta-data of its image. Modern image analysis tools are able to extra the CFA pattern along with other sensor specific details that are useful for understanding a particular camera's behaviour. When analyzing defects, it is important to extract the Bayer pattern of the particular imager-under-test and to analyze the output image accordingly. Knowledge of a particular pixel's CFA pattern helps one to understand defects and potential relations to certain CFA colors.

2.6.2. Image File Formats

Once the sensor captures a scene, it will produce a RAW image. A RAW image is the least treated image format a sensor can output. Processes such as noise suppression and pixel scaling are performed earlier in image collection before the RAW image is formed. Typical RAW images use 12-bit or 14-bits per pixel (i.e. per location). The key point here is the fact that for each location of the RAW image, the value of the pixel represents the intensity of either a red, blue or green location which is set by the sensor's CFA pattern. RAW images do not have any compression applied to them in any

way, making them very large in size. As a result, only DSLR cameras tend to allow direct RAW image transfers for users to access.

A RAW image on its own is not easily viewable and not processed. Most manufacturers have proprietary RAW formats that are not open-source and not easily-readable. The advantage of RAW images is the fact that it gives photographers the most processing control over images before converting them to another standardized image format; typically JPEG. Regardless of the post-processing styles, the very first step in image conversion is demosaicing of the RAW image. The processing pipeline [24] used in digital photography is shown in Figure 2.11. In the processing pipeline there are two noise reduction stages. These stages effectively change the value of the pixel in order to pixel noise due to thermal effects. In defect analysis, this in turn changes the pixel values in the image captures even for RAW images themselves proving to be a challenge when analyzing images for defects. Additionally, these noise reduction stages are not standardized across imagers as each camera manufacturer applies custom proprietary noise reduction algorithms.

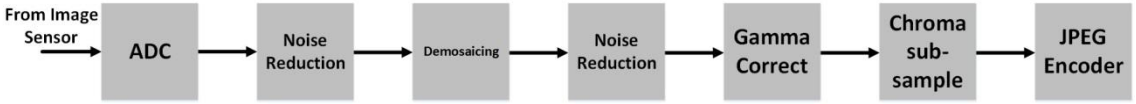

Figure 2.11. Image Processing Pipeline

Demosaicing algorithms are applied in order to reconstruct a full color image from the RAW data using the color scheme set by the CFA pattern. All modern JPEG images undergo this process during their image creation. The simplest version of this algorithm is the interpolation of a pixel's nearest neighbour to obtain the missing color information. As it sounds, this method intuitively uses a 4x4 or 8x8 nearest neighbour technique to average out surrounding pixel values to reconstruct the R-G-B color values at each pixel location while preserving image resolution. However, advanced techniques exist that are designed to avoid image artifacts and reduce conversion noise by iteratively refining the colors. As the complexity of the algorithm increases so does the computational requirements and times. Thus there is a trade-off that manufacturers of digital imagers have to consider when designing software algorithms.

In defect analysis RAW images are the format of choice because each pixel's value is not affected by it neighbours; as mentioned before, RAW images have the least modification. Thus the effect of a defective pixel is isolated to the individual defect site. In JPEG conversion these defects are spread around due to the demosaicing algorithm's interpolation nature, making it difficult to identify the defect pixel location and true intensity. Thus in this research, all experiments make use of imagers that have RAW image capabilities.

2.6.3. ISO

At a high level, the three foundations of digital photography are the ISO, exposure rate and the aperture. The ISO setting of a camera (the exposure index) was developed in the film camera era and is the sensitivity or amplification of the sensor providing a relationship between the exposure time and the output sensor values. The lower the ISO setting, the less the imager is sensitive to the incoming light (or less amplification). For scenes with a high amount of light, a lower ISO setting is used as there is sufficient input light for the image. In low light settings, a higher ISO value is typically used to amplify the incoming light.

When discussing ISO settings, a key point is that the actual pixel photodiode charge accumulation and collection is not affected by the ISO setting itself. The ISO simply acts as a gain mechanism to amplify the output of the pixel. At higher ISO values background thermal noise in the pixel is also amplified which in turn results in an image that is more susceptible to noise, essentially adding a grainy feel to the image. This ISO to noise trade-off must be considered when dealing with digital photography and defect analysis.

In this research the ISO setting is a fundamental experimental parameter for understanding pixel defects. They play a role in the defect pixel output as well varying ISO values in experiments reveal to us behavioural models for characterizing defects. Additionally, defect growth rates and trends are parameterized using the ISO in growth

equations. The hot pixel and SEU defect analyses that will be seen in the following chapters use the ISO setting quite often in discussing their relative defect behaviour.

2.6.4. Standard Pixel Response

When analyzing pixel response characteristics we begin to consider pixels at a higher level of abstraction in which the pixel at a whole is treated as a device. As mentioned in previous sections, each pixel in a sensor is sensitive to the input light and the output response is related to the accumulated time of light exposure on the individual pixel.

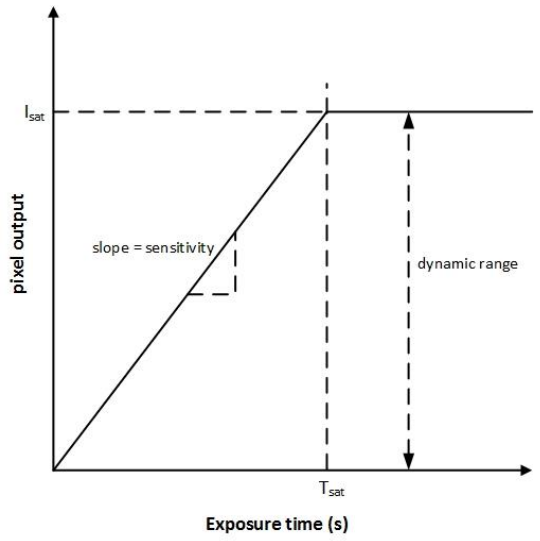

Figure 2.12. Ideal Pixel Response

Figure 2.12 displays the ideal response of a standard imager pixel. This response is characterized by the exposure time and the sensitivity of the pixel itself. Ideally, as the exposure time to light increases, the pixel output will increase linearly up to a max saturation level. The value of this saturation level is also referred to as the max dynamic range of the pixel. The time at which the pixel hits saturation is known as the saturation time, T_{sat}. The response's slope is the sensitivity of the pixel which is directly related to the imager's ISO setting (amplification).

Mathematically, the response of the ideal pixel can is characterized with the following piecewise linear relationship:

$$I_{pix} = \begin{cases} m[R_{pix}T_{exp}] & for\ T_{exp} < T_{sat} \\ I_{sat} & for\ T_{exp} \geq T_{sat} \end{cases} \quad (2.3)$$

The pixel response, I_{pix}, is modelled with slope m (set by the ISO), exposure rate R_{pix} and exposure time T_{exp}. When the exposure time crosses the saturation time boundary T_{sat}, the pixel response is flat. Before the saturation time threshold, the pixel has a linear growth profile. An important concept here is that modifying the ISO of the imager (by changing the internal amplifier gain) will change the response's profile such that the time to reach saturation varies based on the ISO setting. Assuming a constant exposure rate, higher ISO settings reach saturation quicker than lower ISO settings. A depiction of this concept is shown in Figure 2.13 where the pixel response varies as the ISO amplification changes.

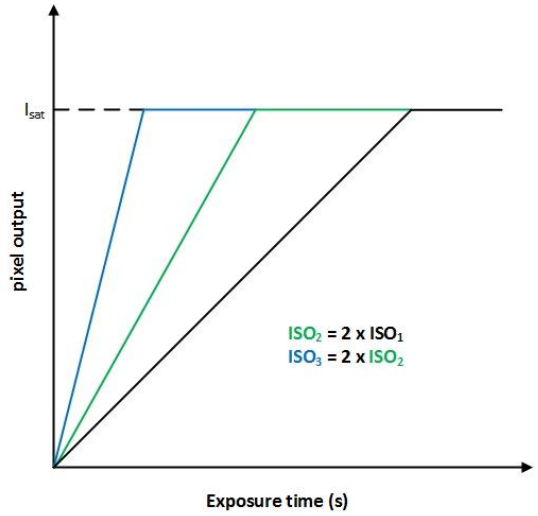

Figure 2.13. ISO effects on pixel response

2.6.5. Exposure Time

The term exposure, as it relates to digital photography, is the amount of light per unit area captured by the image sensor. To quantify exposure, the following relationship for luminous exposure is used:

$$I = Et \tag{2.4}$$

E is the luminance, or total flux, at the surface of the sensor measured in units of lux (lx) and t is the exposure time in seconds (s). The product of these two terms produces the luminance flux measured in units of lx-s. The above relationship is inherently defined as linear with time such that a change in the exposure time changes the total exposure of the image in a linear fashion. Increasing the exposure time will increase the overall exposure which if overexposed, can lead to images that lack edge details due to much light in the image. Similarly, reducing the exposure time will reduce the total exposure but can cause the image to be underexposed leading to muddy looking images. Examples of underexposed and overexposed images can be seen in Figure 2.14(a) and Figure 2.14(b) respectively.

a) b)

Figure 2.14. Examples of (a) Underexposed and (b) Overexposed Images

In digital photography the exposure time is controlled with a setting called the shutter speed which dictates the amount of time the pixel sensor is exposed to the incident light. These shutter speeds are typically measured in units of seconds. Modern DSLRs have shutter speeds as short as 1/8000th of second to as high as 30 seconds (in typical operation) with a range of options in between. In our experiments for defect detection, the shutter speed plays a vital role in characterization of such defects. Given that the pixel values will vary based on the exposure time, the defects will also exhibit different behaviour as the exposure time is varied. Many of the defect models that will be discussed in the future chapters will use exposure time as a key parameter.

2.7. Permanent Defective Pixel Overview

This section will introduce the concept of permanent defective pixels and the various types that exist. For each defect type, the corresponding pixel response curve is displayed.

2.7.1. Defective Pixel Response

In practice, all electronic devices develop defects. Given that the sensor can be treated as a mixed analog and digital device, it is susceptible to developing defects as other semiconductor devices do. Though electrical and material degradation all play a part in defect creation, cosmic rays have been identified as the main source of defect creation through previous research in Dr. Chapman's research lab at SFU [25, 26]. Studies have shown that these defects develop at more rapid rates at higher elevations where cosmic radiation is larger. Figure 2.15 displays a sample 8x8 pixel color image of a grey background. In practice the image should only contain pixel colors that contain the color grey. However, it is clear that a single red pixel in the image stands out and is considered a defect.

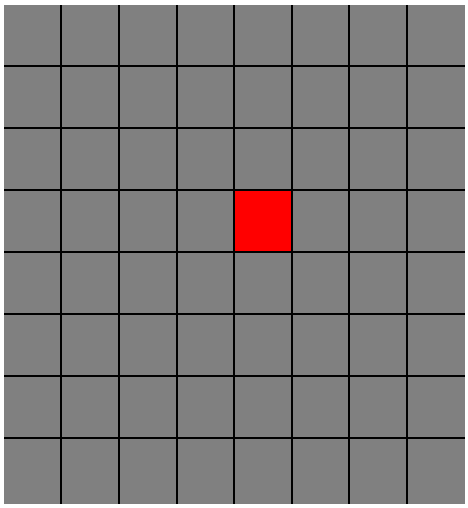

Figure 2.15. Example Hot Pixel Defect

When it comes to hot pixels (permanent defects), the combinations for faulty defect responses are infinite as one could conjure many potential defective pixel response curves. However, past research [27, 28] has identified three main types of permanent defective pixel responses which will be discussed in the next sections.

2.7.2. Stuck Defective Pixels

A stuck defect is a pixel that maintains a fixed intensity value regardless of the exposure time applied. Two types exist, stuck high and stuck low defects. A stuck high pixel will remain max in value regardless of the scene and surrounding pixel responses. Conversely stuck low pixels remain low (or dark). A stuck pixel follows the relationship given in Equation 2.5 where *b* is a constant value.

$$I_{pix} = b \quad for\ all\ T_{exp} \tag{2.5}$$

Stuck pixels are easily identifiable at time of manufacturing enabling manufacturers to map out these defects and bypass them using software techniques. It is important to note that stuck pixels have not been observed to develop overtime for commercially available DSLRs in our research [28] indicating that they only occur at

manufacturing. Hot pixels on the other hand are not easily discernable and cannot be corrected at time of manufacturing.

2.7.3. Standard Hot Pixels

To model the response of a hot pixel, Equation 2.3 needs to be modified to the following:

$$I_{pix} = \begin{cases} m[R_{pix}T_{exp}] + m[R_{dark}T_{dark} + b] & for\ T_{exp} < T_{sat} \\ I_{sat} & for\ T_{exp} \geq T_{sat} \end{cases} \quad (2.6)$$

The above equation adds an additional section to compensate for dark current effects parameterized by the dark response rate R_{dark} and the dark exposure time T_{dark}. An additional offset, *b*, is also introduced and is known as the dark offset. In an ideal non-defective pixel, the R_{dark}, T_{dark} and *b* terms all have a value of zero. In the presence of no light (otherwise known as a dark frame), non-defective pixels will have an intensity response of zero, regardless of the exposure time. This can be seen in Figure 2.16(a). It is important to note that in this figure, the pixel intensity values have been normalized. This normalization of the intensities is a standard way of analyzing pixel curves as it shows general trends on a standardized scale.

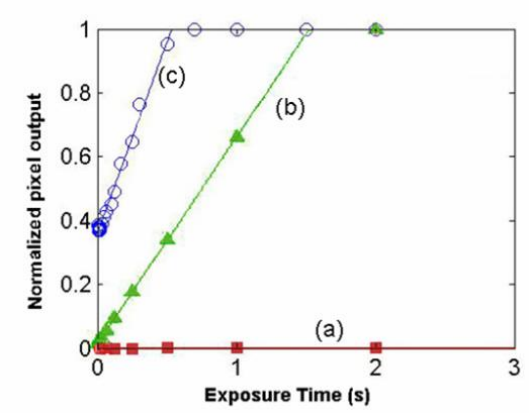

Figure 2.16. Comparing the dark response of imager pixels: (a) good pixel, (b) standard hot pixel, (c) hot pixel with offset [29]

To simplify hot pixel analysis we will assume a dark frame scene in which the light intensity rate term R_{pix} goes to zero. The resulting hot pixel equation now becomes:

$$I_{pix} = \begin{cases} m[R_{dark}T_{dark} + b] & for\ T_{exp} < T_{sat} \\ I_{sat} & for\ T_{exp} \geq T_{sat} \end{cases} \quad (2.7)$$

Again, for a good pixel the above response will be ideally zero as dark current effects are not seen. In practice there is an inherent noise component in the system which means the pixel's value will be in the noise floor and not exactly zero. For a defective pixel, or hot pixel, the above pixel response will have a non-zero R_{dark} term causing an output in the pixels' values in the presence of a dark frame. Using this term we can derive two types of hot pixels. The first being a standard hot pixel and the next a hot pixel with an intensity offset.

The standard hot pixel dark frame response is shown in Figure 2.16(b). This curve resembles the standard good pixel response in a light frame. As the exposure time approaches zero, the effects of this pixel are not seen in the image. While the exposure time increases, the pixel output increases linearly as the dark frame rate also increases linearly with time. Similar to the previous pixel responses seen, the dark pixel also reaches a maximum pixel value at which point it begins to saturate. Thus this type of hot pixel is mostly visible at longer exposures as its initial pixel value is low at smaller exposure times. This is the classic hot pixel typically described in literature.

The second type of hot pixel is the partially stuck hot pixel as seen in Figure 2.16(c). These hot pixels have the same slope, growth and saturation characteristics as the standard hot pixel but have the addition of an offset. This offset is an initial intensity offset at time zero. In theory as the exposure time approaches zero, the pixel output will still contain a significant intensity value. This indicates that partially stuck hot pixels are identifiable at lower exposure time values unlike standard hot pixels. SFU research has shown that in commercial imagers, approximately 70% of the defects are partially stuck hot pixels and 30% are standard hot pixels [29]. Our research suggests that all reported in-field stuck pixels are really partially stuck hot pixels.

It's important to note that though the above defective pixel responses have been analyzed using dark frame responses, their behaviour still exists in light frame scenes. In light frame scenes, the dark frame response will be added to the overall pixel response causing incorrect pixel values. Hot pixels have additional behaviour in light frames which are not strictly linear. There are ongoing studies in this area to model hot pixel behaviour in light frames.

2.8. Hot Pixel Detection

In order to detect defective pixels, specialized software has been developed to assist with this process. This section will discuss the experimental method to detect hot pixels in-field.

2.8.1. Dark Frame Techniques

The hot pixel models that have been presented are characterized using dark frame analysis. There are a few advantages in using the dark frame method over the light frame in characterization and study of defects. Firstly, the dark frame experiment is easy to reproduce as the surroundings are deterministic. Experiments can be done by simply covering the image sensor in a dark room whereas in the light frame it is difficult to accurately reproduce light scenarios when performing experiments. The main advantage of the dark field analysis is the linear nature of the pixel response. Research has been done in analyzing light frame techniques with hot pixels [30] and creating appropriate models. Current papers have found that this behaviour may not be linear and more work in this area is necessary. As a result, this paper will use dark frame techniques for detection and characterization of hot pixels and their behaviour. A key factor that dominates the direction of the dark frame calibration is the system noise in the imager. Even in dark frames the imager is susceptible to thermal noise. Thus at higher ISO ranges this thermal noise is amplified and could appear to be a hot pixel. This in turn limits the amount of significant data that can be captured at higher ISOs.

Additionally, the defect analysis software (discussed in Chapter 3) has been developed in order to take noise characteristics into consideration.

2.8.2. Image Capture Techniques

In this research, dark frame analysis is conducted by covering the imager sensor (typically using the manufacturer provided cover) in a photography dark room or a dark covered box. This ensures no rogue light is present in the experiment environment because with long exposure times, light can leak in via the eyepiece of a DSLR imager. The imager is programmed to capture images in RAW format with all correction and built-in processing tools disabled. Experiments are taken over a wide range of ISOs with increasing exposure times for each ISO setting. This technique enables one to identify hot pixel intensity growth as the exposure time increases for a given ISO setting. A depiction of this process is shown pictorially in Figure 2.17 where the exposure time increases from left to right. This data is then fed into customized software to analyze and output hot pixel behaviour.

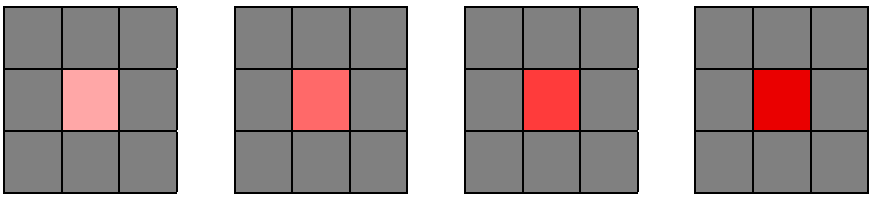

Figure 2.17. Hot Pixel Intensity Increase with Exposure Time

Previous attempts have been made to use JPEG images for defect analysis but have been proved to be greatly ineffective [30]. As mentioned earlier, JPEG images undergo a large demosaicing process that performs color interpolation of the pixels. In dark frame images, this demosaicing algorithm spreads the defect over a much larger area which makes detection of these defects difficult and highly inaccurate.

2.9. Summary

This chapter has outlined the basics of imager pixel and sensor architectures, comparing various options and stating current industry standards. Pixel behavioural models were explored for both non-defective and defective pixels. Specifically, the hot pixel model was introduced for dark-frame analysis. The next chapter will explore software algorithms that are used for analysis in more detail and look at hot pixel experimental data for DSLR and cellphone imagers.

Chapter 3.

Hot Pixel Experimental Results and Analysis

3.1. Overview

The previous chapter presented a foundation on pixel sensor design, digital photography, and hot pixel theory. Specifically, the classical hot pixel model was explained in detail to provide a basis for further research and analysis. The chapter ended with an explanation of dark frame techniques and detecting hot pixels. This chapter will focus on hot pixels from a practical and experimental basis. Firstly, the software algorithms used for hot pixel detection in imagers will be discussed. This discussion is important as it allows one to understand what is considered a real hot pixel in experiments and what data is discarded as noise. Such knowledge is essential as the number of hot pixels detected has a direct correlation with the derived growth rate for a given imager. The concept of defect growth rate will be explained along with the curve fitting techniques used in this research. A key point is that there is very little information in literature on pixel defect rates and how they increase as pixel sizes decrease. This chapter will look at different growth models and how pixel sizes affect the rate.

The main focus of this section and key expansion from previous SFU research will be the analysis of defect rates at smaller pixel sizes. As mentioned throughout this thesis, there is a large push in industry to make pixel sizes smaller for manufacturing and design efficiencies with unknown consequences to defect rates. Additionally, the drastic increase in consumer demand for cellphones increases the trend to push pixels

to smaller sizes. Cellphone imagers and their defect behaviour will be explored in detail along with an updated model of the defect growth rate.

3.2. Hot Pixel Software Detection Algorithms

One can imagine that given the number of pixels in an image extracted from a modern DSLR (10 – 50 Megapixels) it can difficult to manually go through the image and find defective pixels. Thus, there is a need for automated methods for detecting such defects. In this research, a software based algorithm for hot pixel defect detection was developed using a MATLAB based GUI. The process of characterizing defect behaviour for a particular imager involves an experimental lab procedure as well as software analysis processing.

3.2.1. Experimental Process

Before we can analyze hot pixels, the appropriate set of images needs to be captured in order to enable analysis. The process developed involves taking images with the chosen DSLR in a pitch dark environment. Additionally, the camera's lens cover and eyepiece cover are also used to ensure no rouge light interaction is allowed with the camera sensor. The DSLR is setup such that all controllable automated shooting features and additional image processing and correction tools are disabled. DSLRs provide the ability to take images in either manual or automatic mode. Automatic capture mode uses inbuilt software to assist with focusing, exposure control, etc. Manual mode on the other hand allows the user to specify the capture settings such as ISO, exposure time, and other controllable features. For these experiments, the camera is typically put in manual shoot mode capturing the highest quality RAW images. As mentioned in the previous chapter, RAW images are beneficial as the intensity effects on a pixel are not spread to its neighbours. Auto correction algorithms are also disabled during this process. The goal in these preliminary configuration steps is to keep the output pixel values in their most raw state.

A series of images are captured for a sequence of ISO settings for the camera. The ISO range typically starts at ISO100 and increases by a factor of 2 up to ISO6400 – i.e. 100, 200, 400, etc. The aim is to capture an increasing set of exposure times for each ISO setting supported by the camera. The first exposure time is usually 1/1000 second. This initial exposure time was chosen as the initial for two main reasons. Firstly, at this short exposure any stuck nature of the defective pixel, i.e. offset *b*, totally dominates the response. Additionally, at such a short exposure the leakage current, $R_{dark}T_{exp}$ term, in the pixel is small and negligible. One image is taken at each exposure setting. To eliminate an overload in data and RAW files, the exposure times are generally halved as they increased – i.e. the next exposure stop would be 1/500 second, what is known in photography as a one-stop change. The typical upper bound on this exposure setting is in the 2 second range. Between each image capture, there is a 30 second pause that is observed to allow the sensor and camera to cool to room temperature. Additionally between each ISO set, there is a 2 minute pause. Thermal effects on the sensor are random in nature thus waiting a determined amount of time between shots limits the amount of thermal noise in the images.

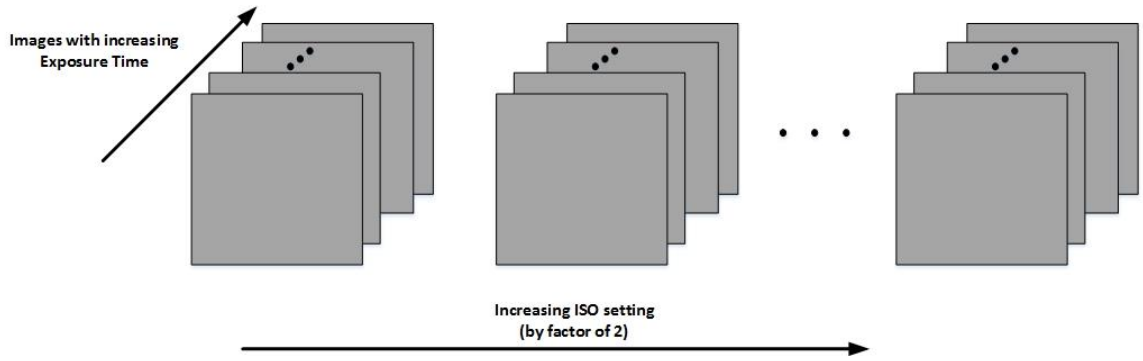

Figure 3.1. Hot Pixel Experimental Process Overview

An overall depiction of the capture process is shown in Figure 3.1. This process is usually referred to as dark frame calibration. For a given date, the camera is calibrated using dark frame images for various ISO and exposure rate combinations. Multiple calibrations are performed over time to produce image sets over time. This enables us to have history of the camera's defect behaviour as times progress. Typically this process is done once every 2-4 months; so about 4-6 calibrations a year. It is also fairly essential

to obtain a calibration set at every beginning of the camera's lifetime (typically after purchase). This initial calibration provides a baseline defect profile at an initial time close to time zero; however, often this is no possible. Once a set is captured for a particular timestamp, the entire set is analyzed using software to extract hot pixel behaviour and counts.

3.2.2. Hot Pixel Detection

Each set of images from a given calibration set are divided into ISO groupings before running the analysis tools. For each ISO there are images with increasing exposure rates. At a high level, the tool does a sweep of all the pixels in each image and compares it to the next image in the sequence (with higher exposure time) to detect hot pixel increases. For example in a set of *N* images for a particular ISO, the current image in the set being analyzed can be denoted as $img_i(x,y)$, where *i* ranges from *0* to *N-1*. For each pixel in $img_i(x,y)$ the software tool will compare the corresponding pixels to $img_{i+1}(x,y)$ in order to extract the pixel value. From this the program will generate a set of hot pixel curves (intensity vs. exposure time) and the number of hot pixels. Additional information such as the pixel color type will also be given. This is done for each ISO setting.

When detecting hot pixels, we need to take into account the noise floor of the image sensor. There will be some fluctuation in the pixel output due to random noise in the system which increases with exposure time. Thus the hot pixel detection tool uses a nominal threshold (typically 5% of the saturation value) to filter out pixels that fall below this threshold as either good pixels or variations due to noise. Another way of looking at this is that the software essentially generates curves for each and every pixel in the image across the exposure time range. At the end of the curve generation the tool will apply the 5% threshold filter on all pixel curves. The majority are filtered out and the rest are considered hot pixel defects.

The concept of filtering using thresholds can be somewhat complicated in that depending at which point a threshold is applied, the amount of data filtered out can vary

significantly. For example, if the 5% threshold was applied at the lowest exposure for a fixed ISO, the majority of pixels would be filtered out as the majority of hot pixels have low pixel values at the smallest exposure time. Only stuck or partially hot pixels will be present after this type of filtering. Conversely, if the 5% filter was applied at the highest exposure, the filter would allow a lot of noise to be collected as potential hot pixels which extremely skews the extracted hot pixel count. Thus, in this research, the hot pixel threshold is applied at the middle exposure to maintain a conservative approach in noise filtration.

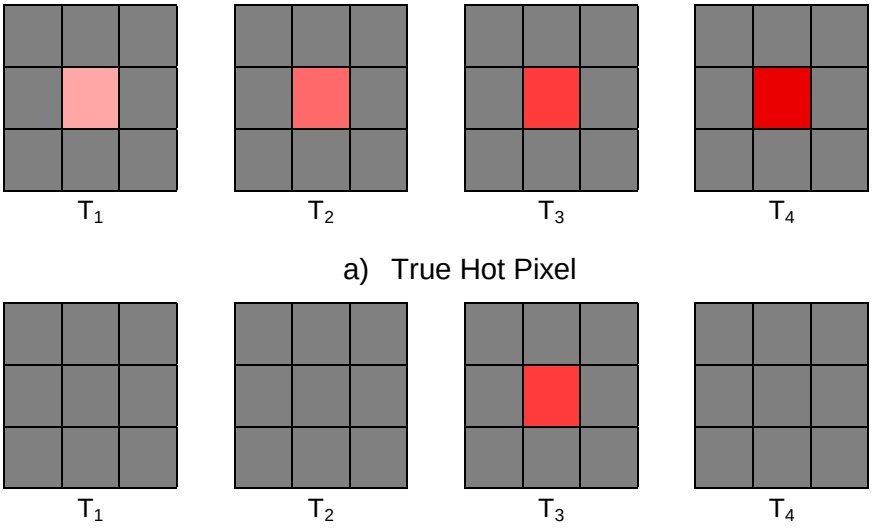

Figure 3.2. Examples of two detected hot pixels

In addition to threshold filtering, the program takes into account false hot pixel detections when running the software analysis. Figure 3.2 displays types of hot pixels that could potentially be collected by the initial stages of the program's detection for a dark calibration image set. Note in this figure, the exposure times are increasing. Figure 3.2(a) displays a hot pixel that starts off with an initial defective intensity but has its intensity increase as the exposure time increases. This is the behaviour of a typical hot pixel. However, Figure 3.2(b) shows a pixel that only has a defective intensity for a single exposure time and is non-defective at other intensities. It is important to note that the pixel in Figure 3.2(b) is not considered a hot pixel but rather an effect of noise or some other transient behaviour. In fact, this pixel behaviour could be considered a

Single Event Upset which will be discussed in the following chapters. In any case, the program will discard this from the hot pixel list.

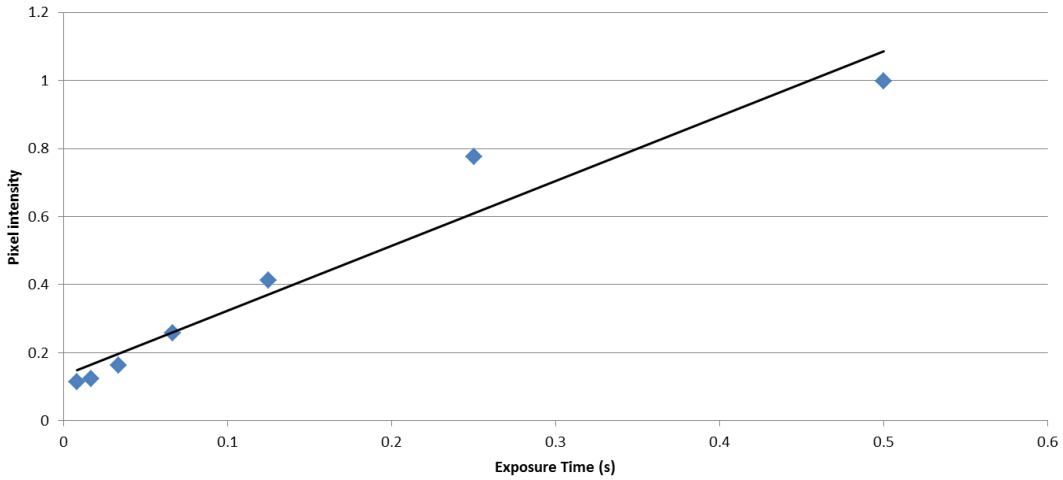

Figure 3.3. Fitted Intensity Curve of a True Hot Pixel (y = 1.9011x + 0.1349, R^2 = 0.9434)

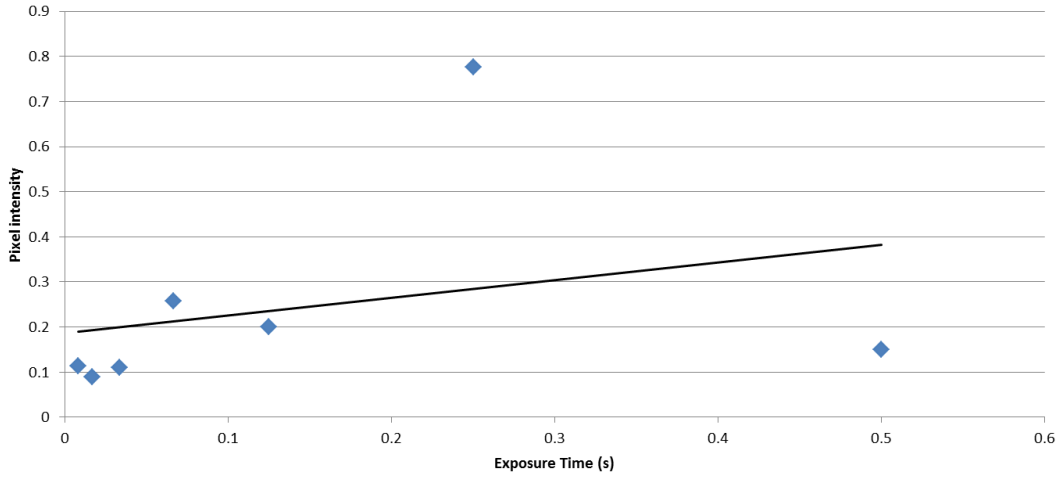

Figure 3.4. Fitted Intensity Curve of a False Hot Pixel (y = 0.3918x + 0.1866, R^2 = 0.0831)

The mechanism through which the detection program discards false hot pixels is a statistical linear regression fit to the hot pixel model shown in Equation 2.6. Figure 3.3 displays the raw intensity values of a proper hot pixel along with its associated regression fitted linear curve. It is clear that the error bounds are within the error of the

respective slope and offset of the regression fit. Thus this pixel would be considered a proper hot pixel similar to the one shown in Figure 3.2(a). In contrast, Figure 3.4 displays the same parameters as Figure 3.3 but for a pixel that would be considered a false hot pixel. From the figure it is clear the second last pixel's error bounds are well out of the error bounds of the curve's slope and offset and would not be considered a hot pixel as is the one in Figure 3.2(b). Mathematically, this can be automated in software by analyzing the error bounds of a simple line equation as show in Equation 3.1:

$$y = b + ax \tag{3.1}$$

In the above equation, the parameters are derived with a regression fit of the raw data. The automated software uses the standard deviation (covariance) on the fit parameters *a* and *b* when assessing whether the pixel is a hot pixel or not. Outliers can be detected by comparing the individual raw data point values to the error bounds of the fitted parameter. For example, if a raw data point indicates a slope value, *a*, that is more than 3 times the fitted slope error, Δa, it is a clear outlier. The same process is applied for the offset, *b*, as well. Mathematically, this can be depicted as shown in Equation 3.2. Relating this back to Figure 3.2(a), it is clear that the fitted slope of 1.9011 is within the error bound of the slope. The same applies to the offset as well.

$$|a| > 3\Delta a \tag{3.2}$$

If a raw data point indicates a slope value, *a*, that is less than 3 times the fitted slope error, Δa, then statistically the possibility of the slope (R_{dark}) being zero is too high for the hot pixel to be counted, as shown in Equation 3.3. Thus the second last data point in Figure 3.2(b) is well outside the error bounds of the fitted slope value of 0.3918.

$$|a| < 3\Delta a \tag{3.3}$$

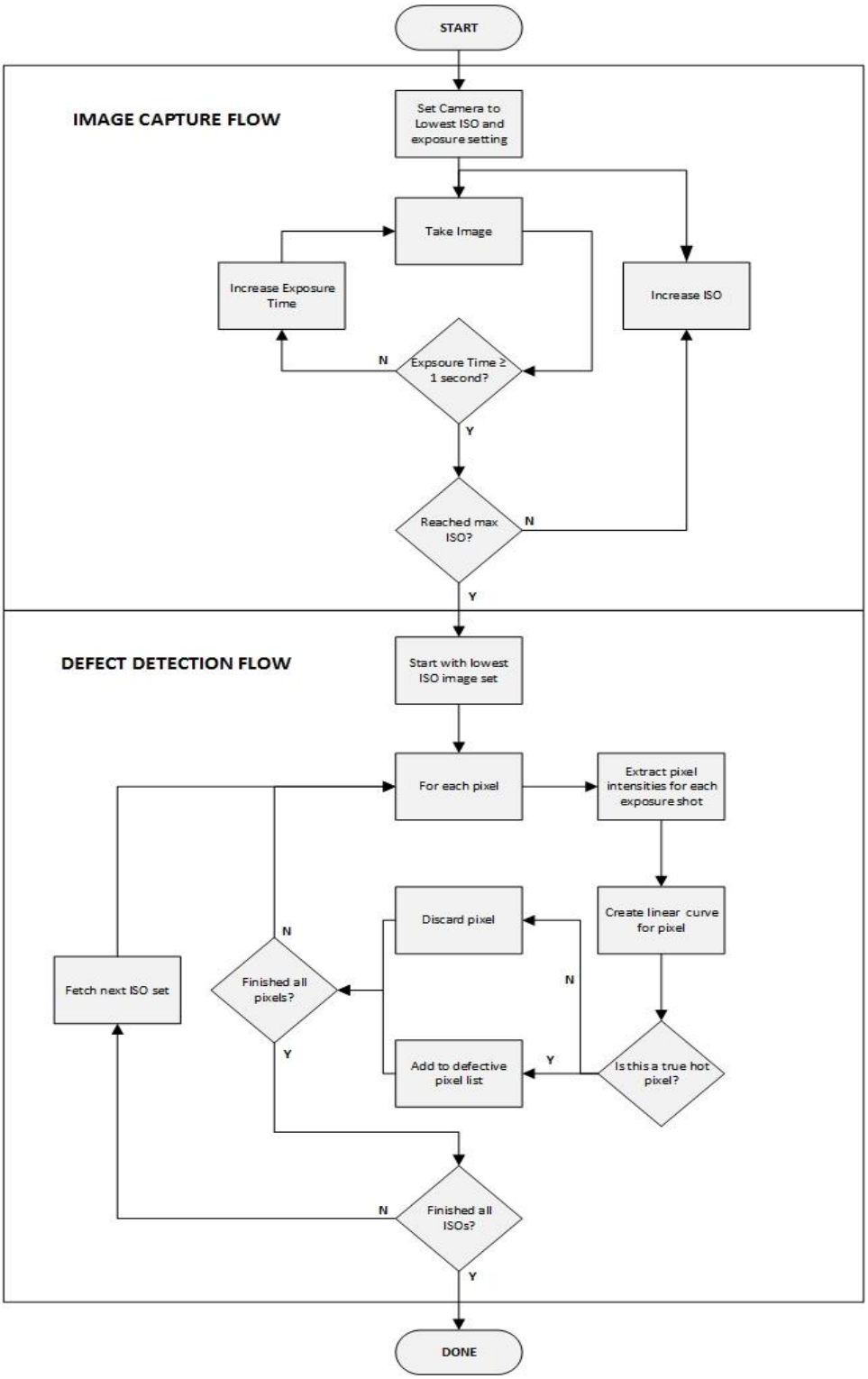

Figure 3.5. Overall Defect Identification Flow

This filtering of false hot pixels is vital as it ensures that the count of defective pixels for each calibration set is accurate without false count increments. These count values are directly used to generate growth rates for imagers over ISO and camera life time. Figure 3.5 displays an overview of the entire defect analysis process. There are two main components of the entire flow – 1) Image Capture flow and 2) Defect Detection flow. The image capture flow consists of the following:

- For a fixed ISO range, capture RAW images with increasing exposure time
- Stop after a 1 second exposure is reached
- Repeat for all ISOs (increase ISO by doubling)
- Once the max ISO has been reached, move onto the Defect Detection process

The defect detection process is done via software. The software extracts defective pixel values and generates hot pixel curves for each ISO set. False hot pixels will be discarded as explained in the previous section. The software portion of the flow is implemented using MATLAB. Other options for implementation exist such as Python scripts, native C++/C# GUIs and other script based options. However, MATLAB possess inbuilt helper functions to ease processing implementation. Specifically, MATLAB has a native image processing toolkit which provides methods to input RAW images and extract/manipulate the associated pixel values. Thus, MATLAB was chosen as the implementation software for this research. The implementation of hot pixel detection methods uses the inbuilt parallelism of MATLAB as compared to nested loops and conditional statements. This provides increased processing performance and aids in extracting values for research. Additionally the use of inbuilt MATLAB functions reduces the processing time for defect detection. To analyze a set of calibration images for a fixed ISO typically takes a few seconds of processing time.

The key advantage of the above flow is that it can be used for any camera that outputs RAW images. In this research, we have used it for cameras from different manufacturers. Additionally, these cameras vary in age, pixel size, ISO ranges and other sensor parameters. The benefit of having one flow is that a standardized research tool can be used that is sustainable as camera technology advances. This eliminates the need of having specific flows based on the camera manufacturer or camera property. RAW images contain a header section embedded in the image file itself which provides metadata such as camera model, image capture date and camera settings.

3.3. Curve Fitting Methodology

The end goal of this research is to develop a relationship between the defect growth rate, sensor size and ISO. The defect numbers from each calibration set can be collected over time for further data analysis. Our research has collected a series of calibration sets for 29 DSLRs over the past 11 years. The end goal is to develop a model of the defect growth rate using the collected data from calibration sets. Various parameters can be used to model the growth rate of hot pixel defects. The two main parameters of interest are the *ISO* amplification and pixel size *S* of the sensor array.

There are various methods that can be used when performing linear regression fits. The most typical method is to use the least squares approach in regression analysis. However, in this research, techniques discussed in [31] are employed. These techniques focus on the analysis of residuals to determine the effectiveness of a fit. A residual is the difference between the actual value and the predicted value of the model. A residual *R* can be defined as shown in Equation 3.4:

$$R = Y_j - F(x_j) \tag{3.4}$$

where Y_j is the j^{th} data point and $F(x_j)$ is the corresponding fitted value. The easiest way to analyze residuals is to plot the residuals versus the predicted values. Figure 3.6 shows an example of a residual plot. The distance from the x-axis to the residual point indicates the deviation between the predicted and observed values. Positive values suggest that the prediction is too low, while negative values indicate an over prediction in the model.

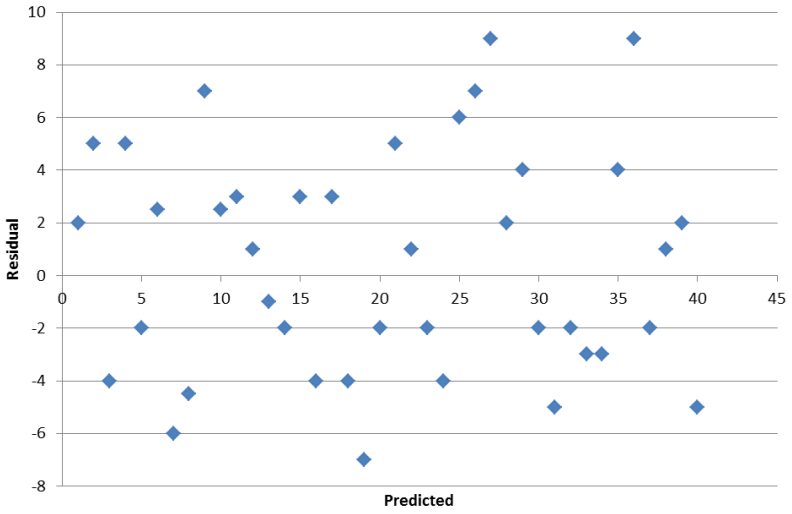

Figure 3.6. Example Residual Plot

Additionally, the general form and pattern of the residual plot can have a strong indication of the statistical significance of the residual plot and the overall effectiveness of the prediction model. Figure 3.7 and Figure 3.8 display examples of two residual plots. The first example shows the following characteristics:

- Residual behaviour is random and not deterministic (ideally, no clear patterns)
- Tend to cluster towards the middle of the plot
- Clustered around lower residual values, not large values (low error)

The above characteristics are what make a favorable residual plot. Figure 3.8 on the other hand shows the following characteristics when analyzing a problematic residual plot:

- Plot is not evenly distributed
- Contains evident outliers
- Clear patterns are discernable

The above basic fundamentals are employed in this research when analyzing residuals. Our prediction models have been highly analysed for residuals with clear patterns, heavy dependence on either x or y axes, and a large number of outliers.

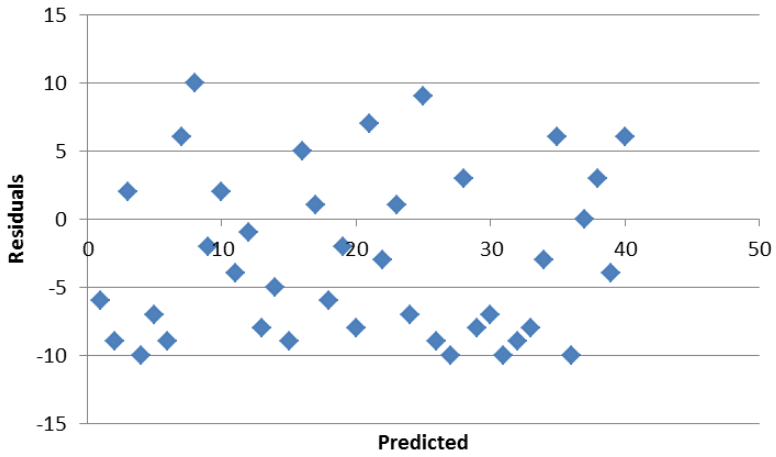

Figure 3.7. Residual Plot Example – Ideal

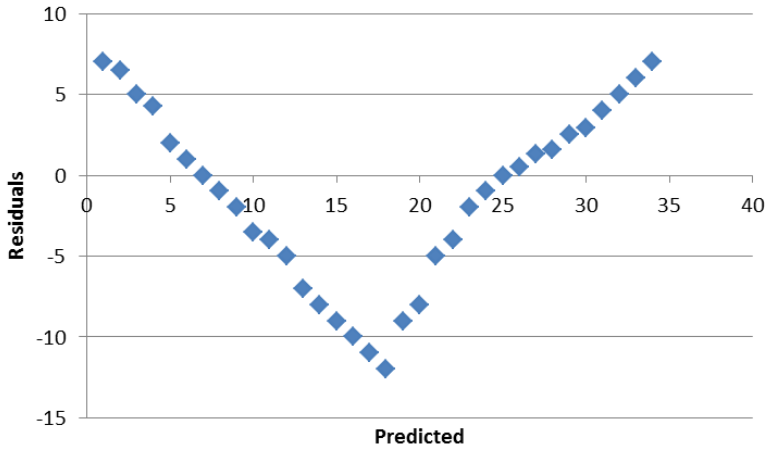

Figure 3.8. Residual Plot Example - Problematic

In addition to analyzing the randomness and behaviour of the residuals, the size of the residuals themselves is important. Figure 3.9 displays residuals that have a random pattern but the value of the residuals themselves is low. This indicates that the corresponding fit is quite good. However, Figure 3.10 displays another set of residuals that show random behaviour with no clear patterns. In this case, the values of the residuals are very large. This indicates that the fit was not effective. When analyzing the residuals from our fits, we take into account the pattern and trend of residuals as well as the residual values themselves.

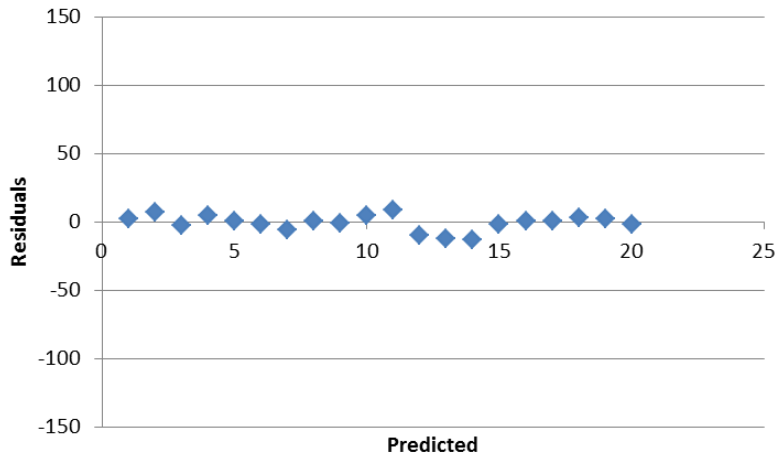

Figure 3.9. Residual Plot Example - Low Error

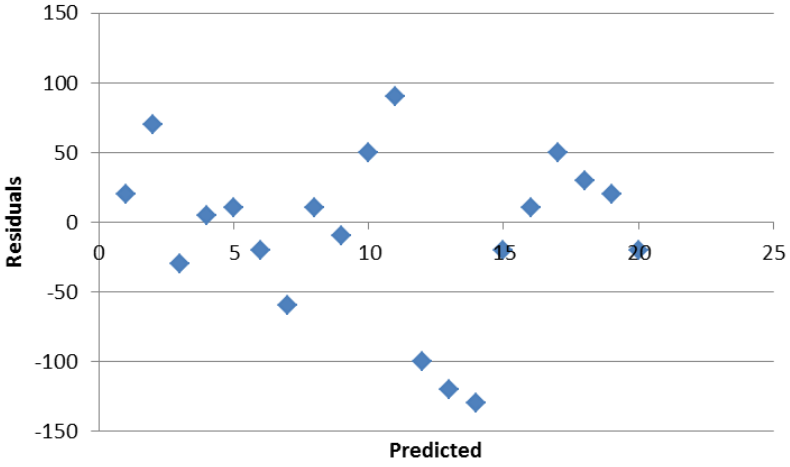

Figure 3.10. Residual Plot Example - High Error

3.4. Hot Pixel Defect Growth Model

This section will discuss the hot pixel growth model and how it was determined using empirical lab data. The statistical concepts and tools that were discussed in the previous section are employed when generating the defect growth model.

3.4.1. Hot Pixel Defect Growth with Pixel Size

It is important to note that when generating linear fit models, data from all the cameras tested for all years is used. This gives us a large comprehensive data set when trying to generate a growth model based on pixel size and ISO. The goal is derive a relationship that would model defect growth as defects/year/mm^2. Before deriving the defect growth relation, initial research [32] focused on generating a rate with a fixed ISO and varying pixel size as shown in Figure 3.11. This showed a linear relationship in the growth trend.

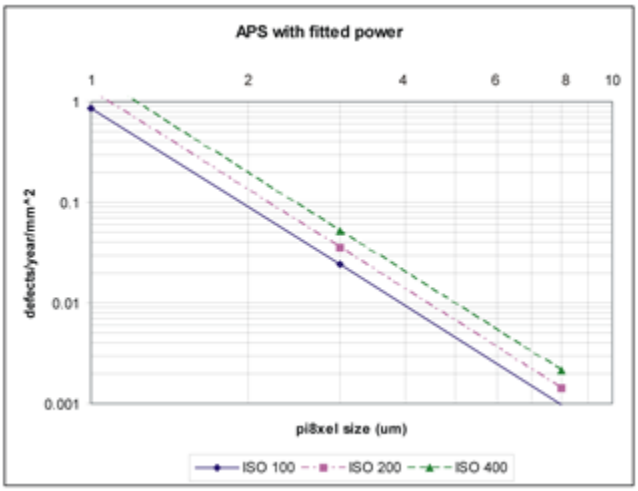

Figure 3.11. APS Defect rate/year/mm^2 vs pixel size for fixed ISO (taken from [32])

From Figure 3.11 it is clear the defect growth has a linear relationship with the pixel size. Additionally, the growth curves for varying ISO have parallel slopes. This strongly suggests that there is an ISO and pixel size relation with the defect growth rate. Thus the hot pixel growth rate needs to take both parameters into consideration.

3.4.2. Power Law

The Oakdale Engineering curve fitting software known as DataFit [33] was used as a tool to search for the best fit relation given the input parameters of ISO and sensor

size. The software suggested a power law form for the hot pixel growth model. For the purposes of this thesis, a form of the power law is as shown in Equation 3.5:

$$D(X,Y) = 10^{A}X^{B}Y^{C} \tag{3.5}$$

X and *Y* are variable members of the power function *f*. These variables will in turn become the ISO and S (pixel size) variables for the growth model. The terms A, B and C are constants that are set based on the linear regression model. The inherent issue with the power law is that it is not linear and very hard to fit and analyze. The term linear here refers to the equation being linear in its parameters (i.e. parameters can be separated). A check for linearity can be done by taking a derivative of the expression in question. For example, Equation 3.5 can be checked for linearity by taking the derivative of *X* with respect to *A*. Clearly the parameters are not separated. However, the above equation can be converted to a simpler form by taking the logarithm of the equation, yielding the following form where the parameters can be separated:

$$\log\big(D(X,Y)\big) = A + B \cdot log(X) + C \cdot log(Y) \tag{3.6}$$

Equation 3.5 is now in a form that can be used for linear regression and curve fitting. Residual analysis is also easier using this logarithmic form. With this knowledge, the hot pixel growth model can now take the following forms:

$$D(S,ISO) = 10^{A}S^{B}ISO^{C} \tag{3.7}$$

The above empirical formula predicts the defect density *D* (defects per year per mm^2 of sensor area) based on the pixel size *S* and *ISO*. Microsoft Excel was used to carry out the data fits themselves.

3.4.3. Hot Pixel Growth Analysis Combining Pixel Size and ISO

Using the empirical relationships mentioned in the previous section, we used the logarithmic form of the power law shown in Equation 3.6 in a least square fit to extract constants to be used in the growth model. Initial research [34] focused on larger pixel sizes (5-10 µm) from mainstream DSLRs. Additionally, separate relationships were developed for APS and CCD sensor types. For a list of APS imagers used in this research, refer to Appendix A. The empirical growth model for APS and CCD sensors is given in Equations 3.8 and 3.9 respectively [34] with the error bounds for the fitted constants shown in Table 3.1.

$$D_{APS}(S, ISO) = 10^{-1.13} S^{-3.05} ISO^{0.505} \tag{3.8}$$

$$D_{CCD}(S, ISO) = 10^{-1.849} S^{-2.25} ISO^{0.687} \tag{3.9}$$

It is important to note that these initial empirical relationships were developed using previous research that used cameras with pixel sizes in the 5 to 10 µm range. The research in this thesis has significantly expanded the pixel and ISO range covered as shown in Figure 3.13. The CMOS empirical formula is generated with the updated hot pixel data which will be discussed in later sections of this chapter.

Table 3.1. Power Law Fitted Constants with Error Bounds

Constant	APS	CCD
A	-1.13 ± 0.26	-1.849 ± 0.22
B	-3.05 ± 0.25	-2.25 ± 0.17
C	0.505 ± 0.081	0.687 ± 0.086

These equations are important as they indicate that the defect rate increases drastically when the pixel size falls below 2 microns. Additionally, the defect rate is projected to reach a rate of 12.5 defects/year/mm^2 at ISO 25,600 (which is available on some high-end cameras). Figure 3.12 displays the fitted power law distribution for APS sensors. Given that the current trend is to reduce the size of pixels, our experimental results project that the number of these defects will increase to high levels, emphasizing

the need to understand how the development rate of these defects increases for even smaller pixel sizes.

A key point to note on Figure 3.12 is that the curve at the lower pixel size (< 2μm) and higher ISO values are shown purely using projected values. At the time the original empirical relation was found (2012), imagers at smaller pixel sizes did not support RAW image capture. Additionally, the usable ISO range was low as higher ISOs suffered greatly from noise issues. Thus the model shown in the figure is purely predictive and projected for smaller pixel sizes and higher ISOs. The following sections will detail the recent push in the industry to smaller pixel sizes and the availability of smaller pixel imagers. Additionally, this research will generate an updated model that will be compared to the original prediction model.

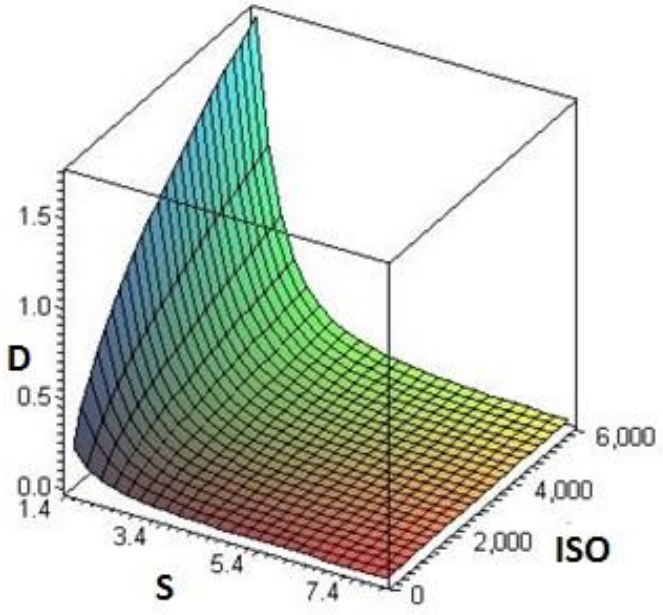

Figure 3.12. Fitted power law for APS defect density (D=defects/year/mm2) vs. pixel size S (μm) and ISO (I) [34]

3.5. Industry Trends to Lower Pixel Sizes

The number of pixels in an average commercial digital camera has increased considerably over the last 11 years. The majority of camera manufacturers have kept the sensor size intact over camera generations but have significantly reduced the pixel size (increasing number of pixels per sensor). This previous research analyzed imagers from DSLR cameras in the higher range pixel sizes (6 - 7 µm), point-and-shoot cameras in the midrange pixel sizes (3 - 4 µm) and cell phone cameras in the small pixel size range (2 - 3 µm). Figure 3.13(a) displays a 3D bar chart summarizing the range of imagers used and data collected in our previous research. On the y-axis, different pixel sizes are displayed (from 8 - 2 µm). On the other, the different ISOs are presented (ISO100 to ISO 25,600). The vertical axis specifies the number of cameras used at a given ISO and pixel size combination. From this figure, it is clear that past research focused on imagers in the larger pixel range and lower ISO settings. The main reason for this is because imagers at the time generally had larger pixel sizes as smaller pixel nodes were not prevalent in available imagers.

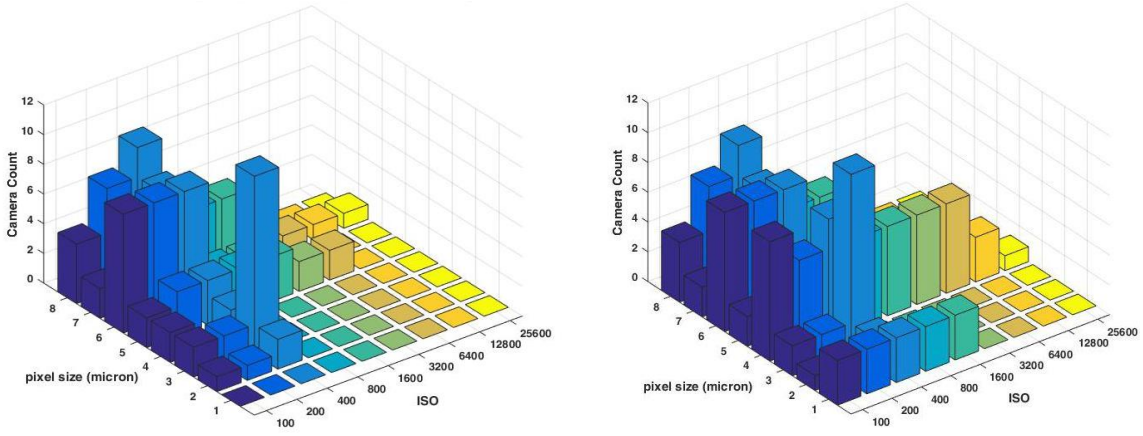

(a) (b)

Figure 3.13. Camera count as a function of pixel size and ISO – (a) Prior: 2006-2012 (b) Current: 2016

The research in this thesis has substantially expanded the data at smaller pixel sizes for many ISOs. An updated bar plot with our current data is displayed in Figure 3.13(b). When comparing Figure 3.13(a) and Figure 3.13(b) it is quite evident that

the research in this thesis puts a greater emphasis on smaller pixel imagers and higher ISO ranges giving us a larger matrix of experimental data for growth analysis and defect rate prediction. The imagers used comprised of DSLRs with smaller pixel sizes (<4 μm) and cellphone imagers. Specifically at the 4 micron range, we have a large increase in the data set for ISO ranges with more coverage on ISOs greater than ISO400. In the past, point and shoot cameras represented the data set at the 4 μm pixel range but in this research we have DSLR camera data at this pixel size range. Even at the sub 2 micron range the ISO range has been enhanced.

One important point to note is that each count on the bar plot represents a larger set of data for that pixel size and ISO combination – i.e. each count represents full dark frame calibration data sets for multiple times and often several years. As mentioned earlier, for each given pixel size and ISO combination we have about 10 data sets (images) ranging from 0.008 sec to 2 sec and conduct a linear regression fit for varying exposure times as shown in Figure 2.13 for each identified hot pixel. Furthermore, each imager contains calibration experiments over multiple times, giving us larger sets of data. Our oldest camera has undergone dark frame experiments at 15 different time points over 13 years, and most have 2 to 5 such periodic measurements. One should also note that Figure 3.13(b) displays a current snapshot and the smaller pixel range will be greatly enhanced in the near future as more imagers become available in this range. In past research we had collected data for both APS and CCD cameras. However as mentioned in previous chapters, CCD sensors are only used in some scientific imagers and have ceased to be used in modern camera manufacturing. Thus our future research will not continue to explore defects in CCD imagers and will concentrate on APS sensors only.

The original defect growth equations in Equations 3.6 and 3.7 were developed using data that was centered at the 5 - 7 micron sizes for the full ISO range, while the smaller number of 3 - 4 micron pixel imagers tended to have ISOs of 100-400. This caused the projection for defect growth at smaller pixels and higher ISO values to have higher uncertainty as there were very few data points in this region when doing the fit. The new data sets shown in Figure 3.13(b) enhance our coverage specifically in the 1 - 4 micron pixel range with higher ISOs in the 1600-3200 range which in turn significantly

reduces the uncertainty of the small pixel region of the curves. In areas where we only obtained a few data points for a given imager, we averaged the rate when doing the curve fitting. For imagers with two or more tests, we did a linear regression for the rate fitting to gain better statistical accuracy. Given that imagers are trending towards smaller pixel sizes, this data will prove to be quite beneficial for imager designers and users. Table 3.2 shows how many sensors of a given area were tested and the types of cameras with those sensors. In terms of sensor area the DSLRs are mostly in the 330 to 350 mm^2 areas, with two at 850 mm^2 (full frame) size. Cell phone cameras ranged from 15 to 22 mm^2.

Table 3.2. Sensor Area for Camera Numbers Tested

Area (mm^2)	Camera Numbers	Type
16	3	Cellphone
23	10	Cellphone
340	18	DSLR
860	2	DSLR

3.6. Cellphone Imager Defect Analysis

The focus of the research in this thesis has been imager defects at smaller pixel sizes (<4 µm). Though DSLR imagers are being designed with smaller pixels, cellphone imagers are the main driving factor in this pixel range. Given high consumer demand, manufacturers have optimized the design and manufacturing of these cellphone imagers at smaller pixel sizes creating the need for study of defects of such imagers.

3.6.1. Enhanced Dark Frame Calibration Methods

The detection and analysis of hot pixels in cell phone imagers is an area where our efforts have been focused as this area of research has not been greatly explored in previous publications and is of growing interest as the application of cell phone cameras increases. This work is important as it reveals how hot pixel generation accelerates as pixel sizes decrease. As manufacturers push cellphone pixel sizes down to 1 micron, our goal is to provide a more accurate estimate of the hot pixel growth rate. Additionally,

given the decreasing cost for cell phone manufacturing, manufacturers do not map out defects at the time of manufacturing, causing higher numbers of imager defects in cell phones compared to DSLR cameras where manufacturing defects are being mapped out. Past research [35] attempted to use 10 identical cell phones of 2.2 micron pixel sizes for calibration tests. However, these phones had very limited exposure controls and would only output images in JPEG format. While we did develop techniques to detect hot pixels, the compressed image format made extraction of the pixel parameters quite difficult and gave low precision.

This area of research requires enhanced experimental methods in terms of image extraction, detection, and analysis, in contrast to what is typically used in experiments with DSLRs. Firstly, the extraction of true digital RAW images from cell phone imagers is quite difficult. RAW image support is not present in most commercially available cellphones. Some variants of the Android OS do support RAW, but only on specific cell phone models and OS versions (5.1 and greater) and then only where the manufacturers have fully implemented the RAW support set. Another complication is that these RAW images are inherently quite noisy which makes identifying and analyzing hot pixels a non-trivial task. In DSLRs, manufacturers apply noise reduction to the pixel data before creating the RAW image as photographers commonly use these files. Additionally, cellphone imagers tend to heat rapidly, due to display and other processing circuitry, thus we need to separate each exposure shot (image) by 30 sec or thermal effects of the sensor will dominate the output image. Other techniques such as turning off the cellphone for a few minutes before doing calibration tests reduce thermal and noise effects in the images. All this is due to the inherent lack of noise suppression algorithms in cell phone imagers as compared to those used in DSLR cameras. As a method to handle these manufacturing limitations, this research has developed specialized detection algorithms that enable us to obtain a defect count for various cell phone imagers. We also ensure that hot pixel detection in cell phone cameras is statistically significant within the error margins. If either the fitted offset or dark current is statistically significant, the hot pixel will be regarded as a true hot pixel. If neither is significant, then it will be considered as noise.

Our initial experimental results indicate that the number of hot pixels that occur in RAW images from most cellphone imagers is very high (ranging between 100 and 500 hot pixel defects) in comparison to DSLR APS defect counts. The majority of cellphone manufacturers do not map out defective pixels at fabrication time, unlike DSLR manufacturers. The consequence to our research is that this requires that we get sufficient measurements over time to do a linear regression back to time zero to identify those initial fabrication time defects. Fortunately (for analysis purposes only), as defect numbers in small pixels increase rapidly over time (e.g., 5 in a month at ISO 400 for 1.8 micron pixels) this can be done with a modest set of measurements over a few months. As more cellphones will switch to newer OS version that support RAW image captures, we will have a wider range of cellphone imagers to analyze for hot pixel defects. Currently, as Figure 3.13(b) demonstrates, we are able to test cell phone cameras with pixels from 1.5 to 1.1 microns, and ISOs from 400 to 1600 ISO. The highest ISOs that each cell imager permits were always found to be way too noisy to extract data from. These small (e.g., 1.1 micron) pixel results showed *D*, defect/year/mm^2, rates that ranged up to 100 times higher than those of DSLRs with 4 micron pixels. This is in line with the power law type relationship of the pixel size we noted in the earlier fits.

3.6.2. Growth Model for Cellphone Imagers

With updated APS data sets using the cellphone imagers, after regression fitting of the power law we have found that the defect rate curve has changed only slightly from the one in Equation 3.6 to the following in Equation 3.10:

$$D(S, ISO) = 10^{-1.12} S^{-3.15} ISO^{0.522} \tag{3.10}$$

The modest changes compared to Equation 3.6 show that the original predicted trends still hold. A comparison of the fitted values between the prior fit and the current is shown in Table 3.3. In fact, the standard errors of the new fitted values are smaller increasing the effectiveness of the updated empirical fit. The Pearson's r coefficient for this fit is r=0.91 which indicates a strong fit and small average errors. A fairly simple technique is used when assessing the quality of a fit. For example, given fit parameter *a*, a_1

represents the first fit and a_2 represents the second fit. Where the error on a_1 is Δa_1 and the error on a_2 is Δa_2. If the difference of a_1 and a_2 is less than 2 or 3 times the sum of Δa_1 and Δa_2, the fit is considered fairly strong. The fitted power of the pixel size S, when taking into account the standard error, is 3.15 ± 0.17, a range that includes the original power law parameters in Equation 3.6 of 3.05 ± 0.25. Note also the standard deviation has reduced.

Table 3.3. Updated Power Law Fitted Constants with Error Bounds

Constant	Prior	Current
A	-1.13 ± 0.26	-1.12 ± 0.26
B	-3.05 ± 0.25	-3.15 ± 0.17
C	0.505 ± 0.081	0.522 ± 0.08

Figure 3.14 displays an updated growth curve based on Equation 3.8. The figure indicates that the hot pixel rate increases by 8.9 times as pixels shrink by a factor of 2, say from 4 microns (current DSLR range) to 2 microns (current cellphone pixel size). Defect rates also increase with ISO to the power of 0.522±0.08 which means that going from ISO 400 to 3200 (a common range now) results in a 3 times increase in the defect rate.

As mentioned earlier, Figure 3.12 showed a curve that had projected values for lower pixel sizes. The updated data in this section makes use of newer cellphones with RAW image capabilities. As pixels decrease to sizes smaller than 2 microns, they have different noise suppression characteristics as compared to traditional DSLR imagers. The initial concern with this change in behaviour is that it may affect the hot pixel growth trend we had modelled earlier. However, as shown, the refined model shows that even with different characteristics in lower pixel sized imagers our initial model trended in the right direction and was within the error bounds of the updated model.

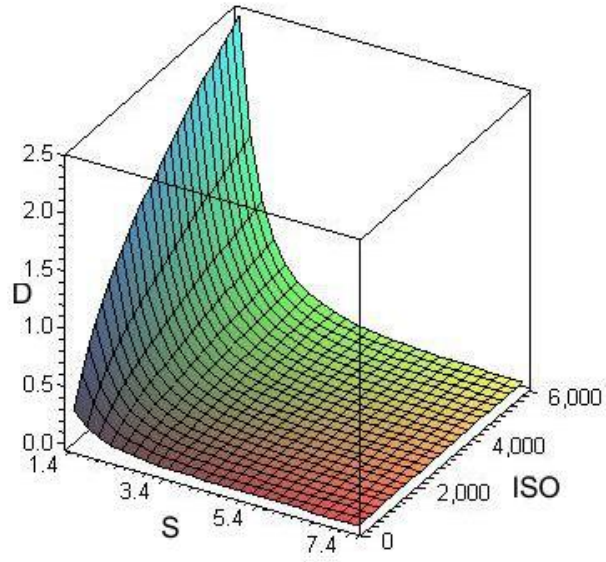

Figure 3.14. Expanded data Fitted power law for APS defect density (D=defects/year/mm2) vs. pixel size S (μm) and ISO (I)

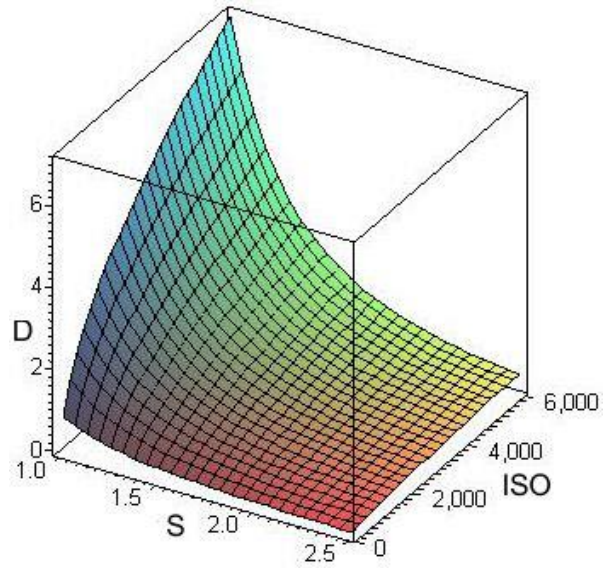

Figure 3.15. Expanded data Fitted power law for APS in the 1 to 2.5 μm pixel range: defect density (D=defects/year/mm2) vs. pixel size S (μm) and ISO (I)

The main areas of interest are the defect rates in the cell phone camera range, which range from 2.5 micron to the 1 micron pixels that manufacturers are aiming at.

Additionally, cell phones are now targeting ISOs of 3200 to 6400 in order to approach the low light capabilities of DSLRs. Figure 3.15 displays how the defect rates will accelerate as 1 micron pixels are approached. Note the vertical defect rate scale is now increased by a factor of 2.6.

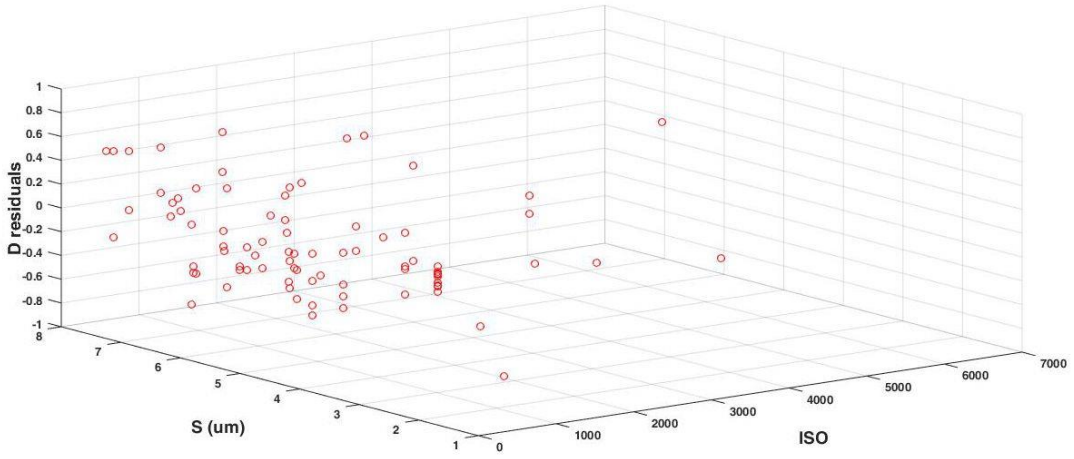

Figure 3.16. Residuals of fitted power law for APS defect density; Residual Log(D) (D=defects/year/mm^2) vs. pixel size S (μm) and ISO

As mentioned in earlier sections, this research uses the distribution of residual errors as an important measure of any fit. As this is a power law relationship we plot the residuals of Log(D) against the pixel size S and ISO. A Log(D) plot is used to avoid biasing to the larger pixel sizes and higher ISO ranges. Analyzing the 3D residual plot in Figure 3.16 shows that there is no evident clustering of the residuals indicating the model is a fairly good fit for the imagers used in this research. For enhanced analysis we observe the residuals against the pixel size S in Figure 3.17, and against the ISO in Figure 3.18. Note that the residuals are quite evenly distributed on both sides of the zero axis for both plots, indicating no systematic deviations with ISO or pixel size S. The residuals at 2.2 microns are clustered on the positive side, but these are all from earlier cell phone tests which only had access to the JPEG images, which had more difficulty in detecting hot pixel, and limited camera control compared to the RAW images used for the other data points. It is noted that the largest deviations are for the high ISO1600 and ISO3200 ranges, though this is understandable as these are the noisiest operating regions of even the DSLR cameras. An important observation with this fit is that our data

in the range less than 4 microns has changed sustainably in contrast to previous research. Additionally, the original data in this area was primarily point and shoot imagers while the current data is predominantly cellphone imagers that differ greatly in technology and software in contrast to point and shoot cameras. However, with this updated data, our fit parameters have changed within the error, giving us a high level of confidence in our fit.

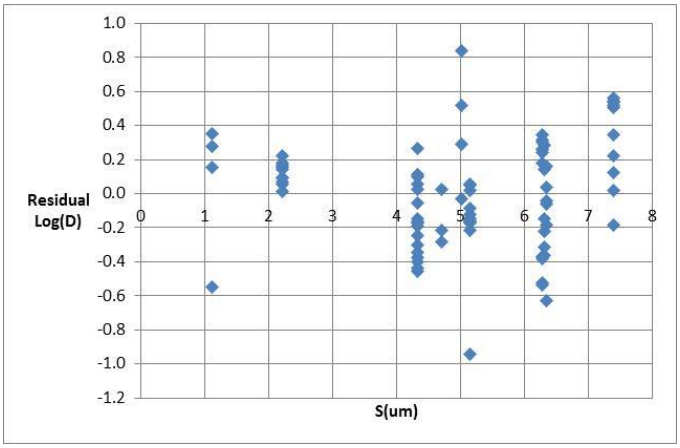

Figure 3.17. Residuals of fitted power law for APS defect density; Residual Log(D) (D=defects/year/mm^2) vs. pixel size S (μm)

Most recent experiments on the smaller 1.4 to 1.1 micron pixels with higher ISO ranges is in agreement with previous projections for the rapid growth of defect rate as pixels approach the one micron size. As a matter of fact, based on our very recent cell phone measurements, these curves are a conservative estimate of the actual defect rate. The fit errors are largest in the smaller pixel sizes, due to the lower number of data points. Specifically, at the 1.1 micron pixels rates of 5.8 defects/year/mm^2 are observed at ISO1600. What is important is that this power law relationship seems to be extending perfectly to the 1 μm range.

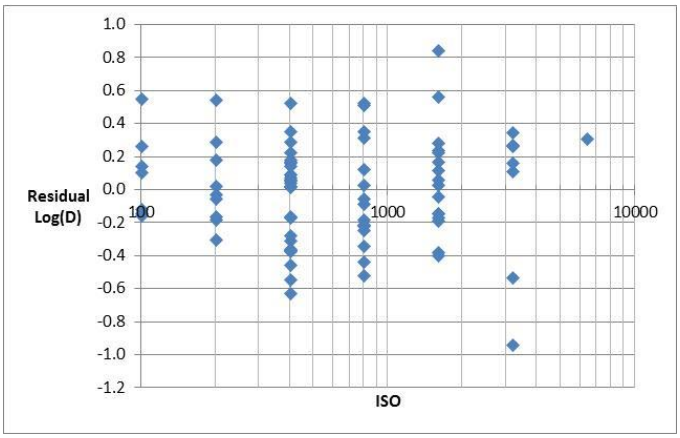

Figure 3.18. Residuals of fitted power law for APS defect density; Residual Log(D) (D=defects/year/mm^2) vs. ISO)

Since the newest generation of cell phones have digital RAW imaging implemented in the OS (Android, iOS), future research expects to significantly expand both the number and accuracy of these data points. This conclusion has important implications for imager designers as they push pixels down to the one micron or smaller pixels. This is further exacerbated by moving ISOs closer to the 6400 or 12,800 values common in DSLRs. The strong indication is that defect numbers will become significant even at these small sensor areas (15-25 mm^2) even with the few year lifetime of typical cell ownership. For DSLR designers, where sensor sizes are typically more than 10 times larger, moving the pixel sizes towards 2 microns will significantly increase their defect rates even with the lower noise sensors available for those cameras. Moreover, the much longer ownership lifetime of those DSLRS, combined with a greater sensitivity of the users to defects, makes this potentially a larger issue for them. With imaging sensors moving into many other products, like car cameras, which have even longer lifetimes (where design targets are for up to 20 years of in field usage), this can have other reliability issues. For example when these cameras are used as part of driving automation, where edge detection algorithms are important, hot pixel growth over these periods can have a significant impact in performance, reliability and safety.

3.7. Summary

This research emphasizes the strong defect growth behavior of hot pixels as pixels sizes are shrunk, especially to the 2 to 1 µm range. Current results show a significant accelerated growth rate in this small pixel range due to the power law relationship with pixel size. The current fits suggest a shrinkage of pixel size by a factor of 2 results in an 8.9 times increase in defect rate. The growth with higher imager sensitivities (ISOs) only increases this effect with a factor of 2 increase in ISO, generating a 1.44 increase in defect rates. Such an increase is of significant importance for DSLRs where serious and professional photographers are very sensitive to significant numbers of defects in their images.

Cell phone cameras, which are the best source of 2 to 1 micron pixels for testing, have just implemented digital raw formats in the past year. Tests showed that using this format was needed for accurate measurements of the hot pixels. Growing numbers of cellphones using this format by the end of 2016 will give us much larger data sets in these small pixel sizes in the near future. These defect rate equations suggest care in the current race for every smaller pixel in cell phones (thus more megapixels) even for these small area sensors shrinkage below 1 micron is projected to produce defect rates that may degrade the image even with the short lifetime ownership of current phones (1 to 2 years). With these clear results imager designers need to take this strong relationship between pixel size and defect rates into account during system planning.

The last few chapters have focused on permanent infield defects in digital imagers. Specifically, hot pixels were discussed and their growth trend. A focus was made on imagers in the smaller pixel sizes including cellphone imagers. In addition to permanent defects, imagers are susceptible to transient or soft defects that are not lasting but have a short manifestation. Traditional ICs experience such behaviour which also includes pixel sensors. The next chapter will explore soft and temporal defects in digital imagers.

Chapter 4.

Single Event Upsets in Digital Imagers

4.1. Overview

The previous chapters focused on sensor design, and permanent defects in digital imagers. Specifically, hot pixel defects were explored in detail and their impact in smaller pixel nodes. In fact, the majority of pixel defect literature has focused on permanent defects. However, image pixels are susceptible to the same transient errors that occur in standard digital ICs. These transient (or non-permanent) defects are known in the literature as Single Event Upsets (SEUs) [36].

The goal in SEU research as they pertain to digital imagers is to study the relationship between permanent and soft errors. In typical digital ICs, the rate of soft errors is much higher than hard (or permanent) errors. Additionally, the question that arises is that given the significant rate of hot pixel defects in standard imagers, what is the rate of SEUs in imagers? Past research in this area has failed to answer this question which could lead to significant sensor design implications. An understanding of the charge levels that are seen in SEU defects also provides insight into hot pixel charge levels.

This chapter will explore our research in the area of SEUs and how they relate to digital imaging systems. General SEU behaviour, experimental detection methods and SEU types will be discussed in this chapter.

4.2. SEU Defects in Digital Imagers

As discussed earlier, over the past several years, our research was focused mainly on the analysis of in-field permanent defects; their development, their characterization, and their growth rate specifically at smaller pixel sizes. Our research has also shown that cosmic rays are the main cause of hot pixel defects.

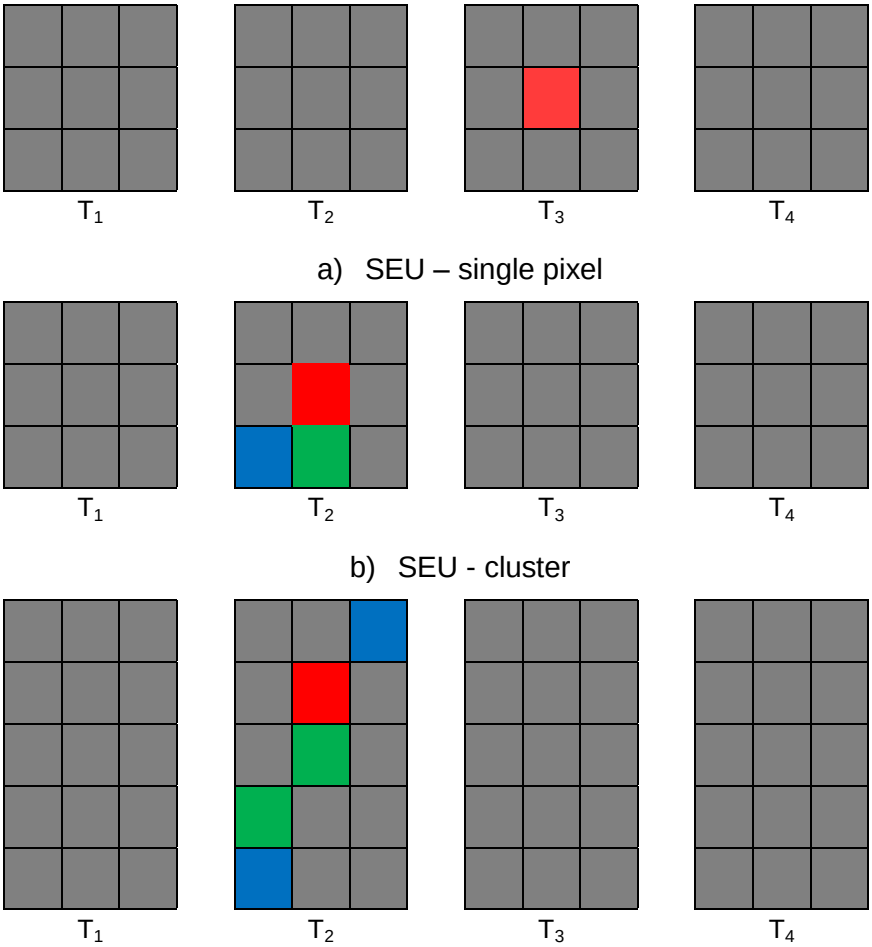

Figure 4.1. Examples of SEUs

Figure 4.1 displays 3 examples of SEU defects. In each case, identical shots are taken with the same digital imager for a dark background. However in certain shots, there are visibly bright pixels (the color of the pixel does not matter). It is important to

note that these defects are only seen for that one image and the defective behaviour is not seen in the previous and next picture, captured at that location. Similarly to other ICs, imagers are also subject to transient defects. These are defects that are seen in-field but are short-lived and therefore appear in only a single image. In this chapter the nature of Single Event Upsets (SEUs) as they apply to imagers will be discussed. SEUs are caused by cosmic particles that strike the imager at random times and locations. Depending on the particle energy, the SEU can deposit charge to cause a soft error that can be seen in the actual values collected by a pixel. In modern literature there has been considerable study of SEUs as they relate to digital ICs [37].

More recent research has started to look at SEUs in digital imagers, including the use of cell phone sensors as detectors for cosmic ray activity [38]. Unlike standard digital ICs, pixels in a digital imaging sensor can be monitored at almost any desirable frequency. Since a SEU manifests itself as one or more brighter pixels in an otherwise dark image, the rate of SEUs can be measured at a considerably higher accuracy by taking dark-field pictures at different exposure times and different frequencies. Another difference between the imager sensor and traditional ICs is that image sensors provide us with location and charge/energy data, charge spread and rate when analyzing defects.

In digital ICs it is known that SEUs occur typically at about a 100 times greater than permanent faults. In these ICs, the SEUs are hidden and difficult to locate. However, the SEU rate (or number of temporarily erroneous pixels) as compared to the rate of permanent hot pixels in digital imagers has not been discussed. This is important as it helps understand the effect of these temporary defects at different ISO/exposure times and also enables camera manufacturers to better design for reliability and fault tolerance. Therefore, the understanding of image sensor behavior in the presence of SEUs is vital.

One important point to highlight is that the design methodology taken by digital camera manufacturers is inherently much different than traditional digital IC manufacturers. In modern day digital ICs, a lot of added circuitry and protection is

designed into the chip to avoid and correct soft errors. In high speed bus protocols the use of data parity and CRC protection is quite common to detect soft errors and potentially correct for them. Additionally, most RAM designs in today's digital circuits contain enhanced ECC protection that can correct single-bit ECC errors and detect higher bit errors. In systems where high speed DSPs are used, manufacturers stress circuitry in order to reduce the bit-error-rate (BER) value to levels where advanced error correction coding can correct soft errors. Digital imagers are much different in nature; hence our research is looking at SEUs in imagers first as a tool to better understand SEUs in ICs.

Most of the past research that has taken place in this field has focused on cosmic ray detection and analysis in imager sensors. In essence, SEUs were observed and analyzed at a transistor physics level. The goal of this research, on the other hand, is to study the decrease in image quality resulting from the imager defects, with an eye towards developing defect mitigation techniques. Clearly image quality depends on the image's exposure time and ISO setting, so our results can allow camera manufacturers to improve the reliability of their designs. We will look at the results of our experimental study of soft and hard errors in digital cameras.

4.3. SEU Defect Detection Methods

Unlike hot pixel defects, SEUs are not permanent indicating a new detection algorithm is needed when attempting to identify defects. This section will explore the experimental process behind detecting SEUs and various noise considerations that were taken into account.

4.3.1. Experimental Overview

In order to identify SEUs, we used DSLRs as our first test devices because they have large imager areas with highly sensitive pixels, and allow direct access to the pixel

RAW values without image processing such as jpeg that tends to distort the data [39]. The experimental method for this research differs from what was used in the hot pixel research. For the hot pixel experiments, a series of images were taken at increasing exposure times with a fixed ISO. Then a linear fit was performed in order to create a curve as shown in Figure 2.13. However, for the SEU experiments the important issue is total accumulated exposure to events; hence, we took a series of medium to long exposures (1 to 30 seconds) at a fixed ISO. Because the exposure time for each image is fixed, this allows us to look for events the only occur in a single image and then go away. The key point is that SEUs are by their nature very short in duration and suddenly inject a charge into the local area of the IC. However, in digital imagers the pixel integrates charge changes over the duration of the exposure, and by taking an exposure of a given duration the imager records both the temporal and spatial occurrence of each SEU even if the SEU disappears. Still, we could not take very long exposures with digital cameras as they accumulate noise in the image (e.g., thermal generated electrons) over time. The maximum exposure time varies with the camera and the ISO but is typically in the order of 10 to 30 seconds before noise becomes so prevalent that identifying SEUs is difficult. Hence, in our experiments we needed to take a sequence of short duration images.

In order to reliably measure the effect of SEUs on imagers for various operating conditions, we created an experimental setup to collect a large number of dark-frame images. Effectively, these images needed to be precise temporal snapshots of the sensor activity for a specific time period at various camera settings: ISO levels and exposure times. The sequence of images also allows us to separate SEUs from the hot pixel events and obtain a temporal rate for these short duration events.

In designing the experiments we first used a camera with a large imager (36 by 24 mm^2) and a high sensitivity (ISO) which previous research showed would develop about one hot pixel every 12.5 days. This camera had support for RAW image output. Based on the reported ratio of 100 SEUs for each permanent fault, we expected to have to take a large number of pictures before detecting a noticeable number of events. In practice it turned out that SEUs were more common than we expected, and our setup resulted in a significant number of detections.

In order to take multiple shots at a fixed ISO and exposure time, we made use of a digital camera remote control, called an intervelometer, which would take a set sequence of images. The remote was set up such that after each shot (image), a one minute delay was inserted to remove any effects of thermal noise caused by the sensor heating up as the experiment progressed. 3 types of intervelometers are available for use in modern digital camera technology:

- Self-contained intervelometer – this is a remote device that plugs into the camera's control port. The remote intervelometer has settings for capture duration, interval wait time, and number of images to capture. The advantage of this method is that an external computer is not required for image capture.
- Software controlled – most DSLR manufacturers provide software that allows one to control camera shooting via a USB interface to the camera itself. This method has the benefit of being able to save images directly to the computer's disk drive rather than the camera's memory card.
- Built-in intervelometer – more recent cameras have built-in timed shooting features that mimic the external intervelometer. Again, the advantage of this method is that the experiment is portable and does not rely on a computer. However, this tends to use more camera battery as the remote shooting features are now in the camera itself.

On average, a set of 150 to 250 images was collected for each ISO and exposure time combination. The above image number was set by the maximum picture limit of the camera batteries or the memory card itself.

It is important to note that these experiments were all conducted in a pitch dark room or box so that no incident light fell onto the camera sensor. This enabled us to detect any temporary defects caused by SEUs.

To analyze the images for SEU artifacts, a software tool was created. This tool read in the RAW images and executed the following algorithm using 3 consecutive images at a time (as shown in Figure 4.2):

- Flag any pixels that have a pixel increase from image j-1 to image j using a predetermined threshold
- Using the pixel locations from the previous step, check to see if any of them have a decrease in pixel values from image j to image j+1 using the same predetermined threshold

- If any pixel location satisfies the above conditions, it is marked as an SEU defect location

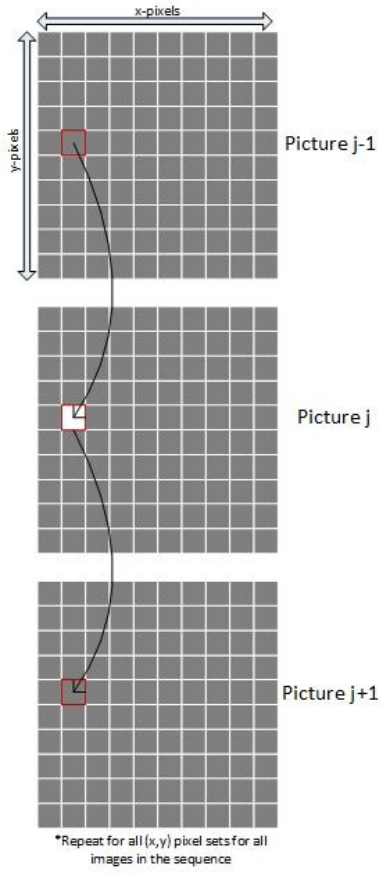

Figure 4.2. SEU Detection Algorithm demonstrating an SEU that was detected in image 'j' and not present in images 'j-1' and 'j+1'

This algorithm ignores locations where known hot pixels resided. Given our previous research with hot pixels on this particular imager, the hot pixel locations were known and were not used in the analysis in order to avoid any false positive results.

As with the hot pixel analysis software, MATLAB was used to implement the SEU analysis software. Unlike the hot pixel analysis case where the software dealt with a handful of images at a time, the SEU analysis requires all images to be imported at the time of analysis. This means that the software could be storing 250 images worth of pixel data in memory implying that the overall coding implementation will greatly affect software performance. Our initial revision of the MATLAB software used nested loops

when analyzing pixels across horizontal and vertical directions while comparing pixel values. Though this performed the actual analysis correctly, the performance was quite poor in that it took about 2 hours to analyze 100 images for SEU defects. In general, most experiments resulted in 500-1000 images and gigabytes of data which makes processing efficiency important. Given the poor performance results, the SEU analysis software was upgraded to use parallel processing features built into MATLAB. These features inherently provide the same functions that were previously implemented with nested loops; however they make use of lower level MATLAB code benefits to provide increased performance. For example, instead of looping through each pixel in the image, the 'find' command was used to locate pixels that were above a certain value. Using these code enhancements, the processing time for 100 images reduced to about 5 minutes which is a significant increase. The SEU analysis software does not make use of GPU processing tools but rather the standard CPU threads. Future research will make use of more complex GPU libraries for increased processing speed and throughput.

4.3.2. System Noise Consideration

An important concern that arises with any experiment is the validity and repeatability of results as they relate to system noise. In the SEU experiment case, one can imagine that fluctuating system noise in the imager could potentially lead to the above algorithm flagging noise fluctuations as SEU locations. In order to get a baseline for the noise in our system, we took a series of images at each ISO and exposure setting to better analyze the noise levels we were dealing with. For each ISO and exposure setting combination, 5 images were taken in a pitch dark room. The pixel values were then averaged to collect the mean noise floor for the imager. These are displayed in Table 4.1.

Table 4.1. Averaged Baseline Noise Values

	ISO 400	ISO 800	ISO 1600	ISO 3200	ISO 6400
Exp. Time (s)					
0.5	~ 0	~ 0	~ 0	0.01	0.09
1	~ 0	~ 0	~ 0	0.01	0.10
2	~ 0	~ 0	~ 0	0.01	0.10
4	~ 0	~ 0	~ 0	0.02	0.12
8	~ 0	~ 0	~ 0	0.03	0.15
15	~ 0	~ 0	0.01	0.07	0.23

In the images captured, pixel values can range from 0 to 255. A pixel value of 0 indicates a completely dark location while a value of 255 represents a fully saturated one. Clearly from the above images, all the averaged noise values are very low and negligible for even the highest ISO and exposure time combination. Additionally, when the averaging was done, locations with known hot pixels were not included in order to avoid false analysis. Overall, the noise in the imager system is not a concern and our SEU analysis algorithm will prove to be effective in detecting defects.

4.4. SEU Defect Classification

Figure 4.3 displays the three main types of SEU defect types. The first being a single spot event (bottom), the other a streak event (top left) and the last being a cluster event (top right).

A simple SEU spot is a single pixel location that accumulates charge due to an incoming cosmic ray or energy source as seen in the bottom pixel shown in Figure 4.3. This value is then collected by the digital imager's processing circuitry and eventually makes it onto the image itself. The key point here is that the SEU event is isolated to one pixel and not spread to its neighbouring pixels. Additionally, Figure 4.3 displays an SEU cluster at the top right of the image. This is where the SEU event is between multiple pixels and the charge is spread creating an 'L' type structure.

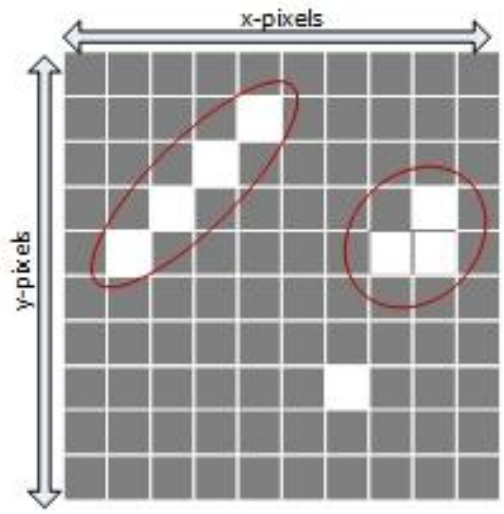

Figure 4.3. SEU types – simple SEU spot (bottom), SEU streak (top left) and SEU cluster (top right)

More complicated SEU manifestations are possible and are known as streak defects. Streak defects involve a number of neighbouring pixels in the defect behaviour. It is important to note that the defect itself is still caused by a single cosmic ray energy event but the effects are seen over a range of pixels in the vicinity. Figure 4.3 shows an example of a streak event at the top of the image. In this example, a cosmic ray particle caused a group of pixels to exhibit defective pixel values. The collections of pixels in this case are considered as single SEU event in our detection algorithm. Figure 4.4 and Figure 4.5 display actual experimental SEUs from infield images in these tests. More examples and details will be explained in the following chapter.

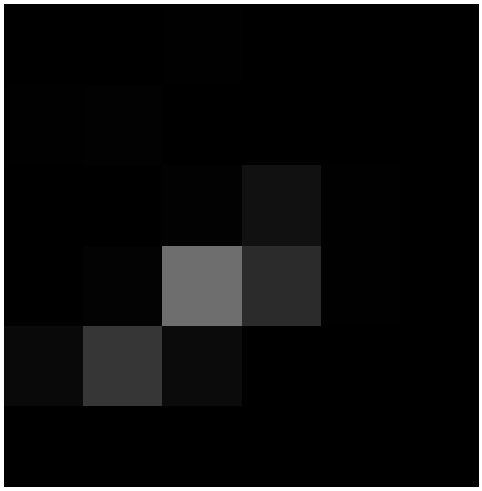

Figure 4.4. Experimental SEU Streak 1

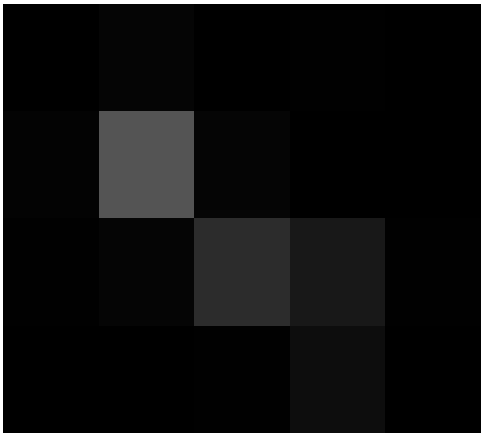

Figure 4.5. Experimental SEU Streak 2

In regular ICs the SEU on a given circuit element is often hidden behind the surround circuit operations so that both the physical location and actual charge deposited are hard to characterize. Studying SEUs in digital imagers is considerably simpler as it can be done by taking dark-field photos at a high frequency and long exposure times (up to 30 seconds). The instant an SEU occurs, the charge it deposits is captured as a bright dot in the picture and is retained by the pixel even after the SEU disappears allowing the determination of the physical location and the charge generated. The next chapter compares the hot pixel rate to the SEU rate to better understand the permanent hot pixel generation process.

4.5. Summary

This chapter has explored the theoretical concept of SEU defects in digital imagers and the motivation for this research. The lack of publications and literature that focus on transient errors in digital imagers with respect to image quality leads to a greater need for this area of technology to be explored. The next chapter will discuss our experimental results and analysis for SEUs in CMOS imagers.

Chapter 5.

Single Event Upsets Experimental Results and Analysis

5.1. Overview

In this chapter the results of our SEU experiments will be analyzed. Unlike standard digital ICs, pixels in a digital imaging sensor can be monitored at almost any desirable frequency. Since an SEU manifests itself as one or more brighter pixels in an otherwise dark image, the rate of SEUs can be measured at a considerably higher accuracy by taking dark-field pictures at different exposure times and different frequencies. A range of imagers will be used in the analysis.

5.2. Experimental Results

Using the SEU detection algorithm mentioned in the previous chapter, we conducted experiments at different ISO and exposure times to collect SEU defect counts. One important thing to note is that the camera that was used for this experiment was set-up such that no image post-processing was introduced (i.e. RAW images were used). RAW images are the minimally processed pictures that essentially contain pixel data as taken by the camera. There are minimal processing algorithms or demosaicing performed on the RAW images because color is unimportant at this level.

As a starting point we began at ISO 6400, performing experiments at 30s, 10s, 3.2s and 1s. For each experiment about 100 images were taken. The initial expectation was that digital imagers would experience about 100 times more SEUs than typical ICs. Thus, given the known hot pixel defect rates, the theoretical expected runtime to hit such an event is around 24 hours. However, during our initial experiment at ISO 6400 with a 30 seconds exposure, we observed many events in the first hour itself (almost one every 10 seconds). Also, in our first set of experiments, we have discovered several interesting forms of SEU defects, specifically SEU streaks as mentioned in Chapter 4. An example is shown in Figure 5.1. In this example, an incident cosmic ray has hit the imager, depositing a charge covering 5 neighboring pixels in a line. We consider this a single particle hit as the cause of this streak is likely a single SEU. We justify this by noting that the event rate (at most a few SEUs per a 21 megapixel image) is such that the probability of 5 events occurring as neighbors is extremely low. Moreover, such streaks turned out to be a common occurrence. These streaks are really the charge equivalent of the trails left by cosmic ray particles in classic cloud chamber detectors.

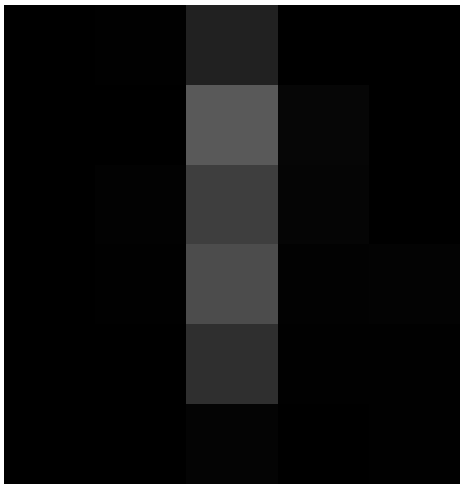

Figure 5.1. Simple Experimental SEU Streak (snapshot of 5x6 pixels – 31.3µm x 37.6 µm)

A more complicated streak is shown in Figure 5.2. In this example, it is clear that the incident cosmic particle began at a particular direction. However, at some point, it incurred a deflection. One possibility is that the incident cosmic ray particle collided with an atom, causing the particle to deflect and creating this interesting SEU defect. From

the figure it is clear that there are gaps in the streak which are likely due to some pixels not accumulating enough charge from the incident particle to show the SEU brightness.

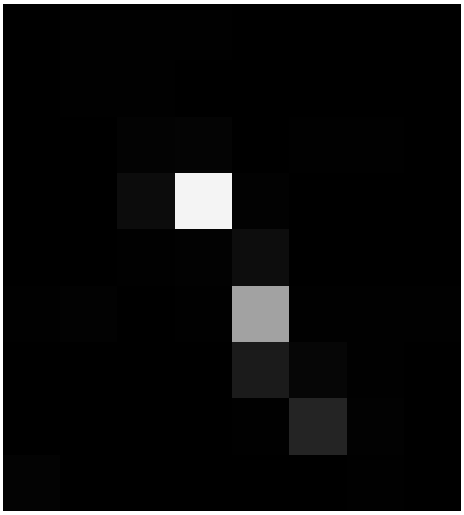

Figure 5.2. Complex SEU Streak (snapshot of 12x17 pixels in size – 75.12µm x 106.42µm)

With this complex observation of streaks with inherent gaps, we upgraded our algorithm to consider a streak as a single SEU hit. This method also took into account streaks that had gaps. This enables us to effectively treat an SEU that created a multiple streak as one single event.

5.3. SEU Analysis

Using the data obtained by our experiments we can now attempt to define certain trends and rates of SEU growth at various operating conditions of the imager. We have counted SEUs that appear in streaks as a single defect as shown in Figure 4.3. Figure 5.3, Figure 5.4, Figure 5.5, and Figure 5.6 display the defect count distribution for each exposure time for the ISO 6400 experiments. A Canon 5D Mark II DSLR with a pixel size of 6.26 µm was used for these experiments. From the distributions we can see that each of the exposure time set has a clear peak value. Additionally, at the ISO 6400

with a 30s exposure time case, we see that every single image contained an SEU; there was not a single case of no SEUs being detected.

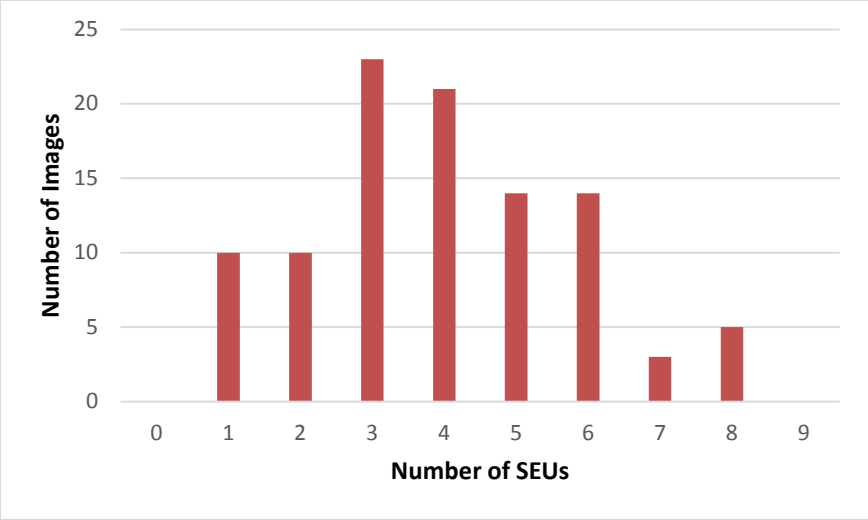

Figure 5.3. Distribution of SEUs per image (ISO 6400, t=30s) – Canon 5D MII, 6.26 µm – Peak ~ 3 events/image

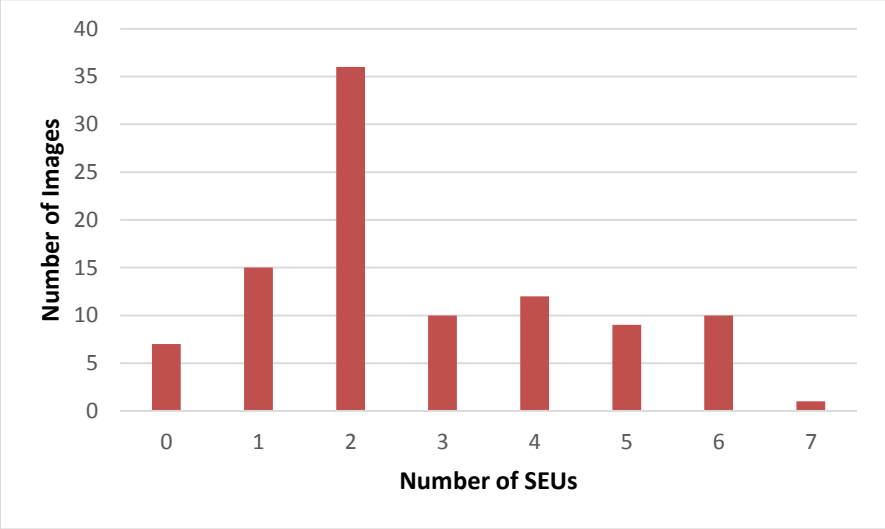

Figure 5.4. Distribution of SEUs per image (ISO 6400, t=10s) – Canon 5D MII, 6.26 µm – Peak ~ 2 events/image

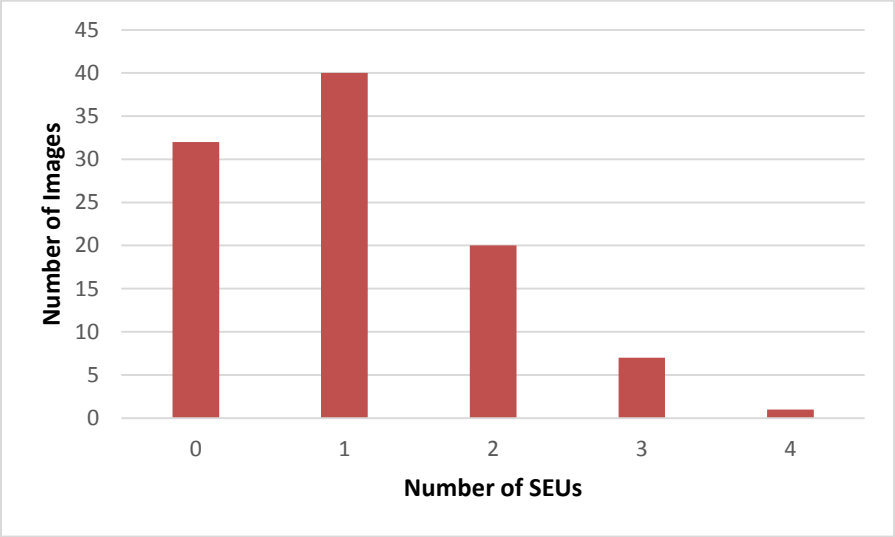

Figure 5.5. Distribution of SEUs per image (ISO 6400, t=3.2s) – Canon 5D MII, 6.26 µm – Peak ~ 1 event/image

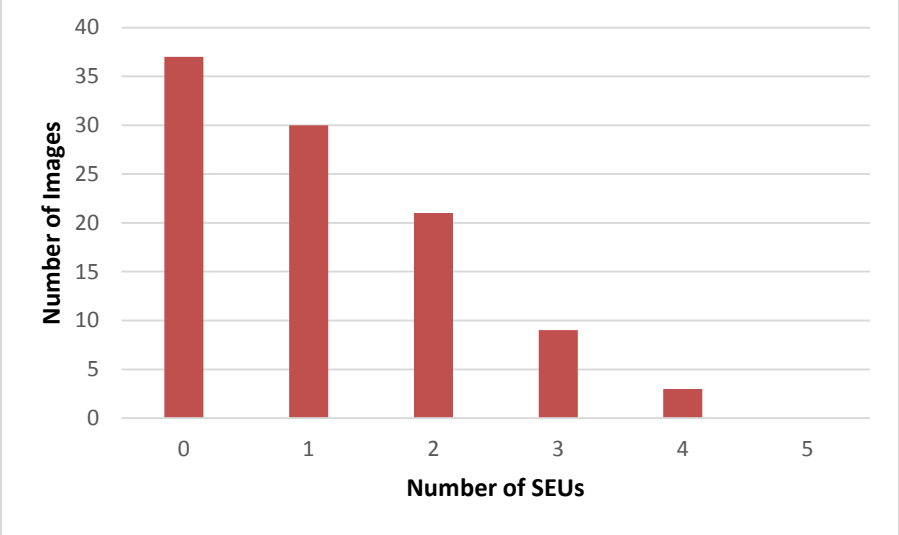

Figure 5.6. Distribution of SEUs per image (ISO 6400, t=1s) – Canon 5D MII, 6.26 µm – Peak ~ <1 event/image

In order to understand the dependence on ISO, the same tests were repeated with ISO1600. These distributions are shown in Figure 5.7, Figure 5.8, Figure 5.9, and Figure 5.10. The distributions here are similar to the ISO 6400 case except that the peak SEU counts now occur at lower values as we would expect when we lower the ISO

setting. Additionally, in each of the exposure time experiments at ISO 1600, we see cases where images did not contain SEUs.

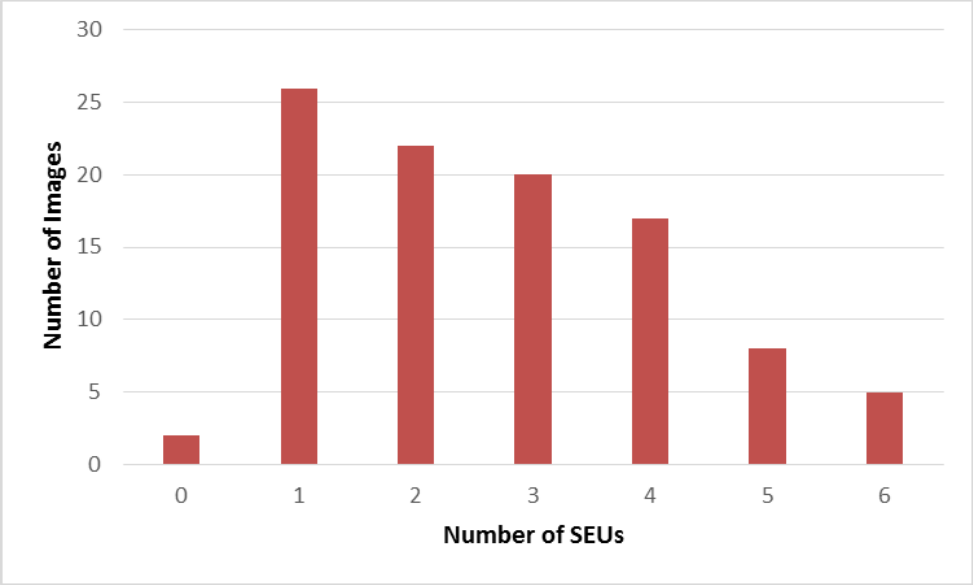

Figure 5.7. Distribution of SEUs per image (ISO 1600, t=30s) – Canon 5D MII, 6.26 µm – Peak ~ 1 event/image

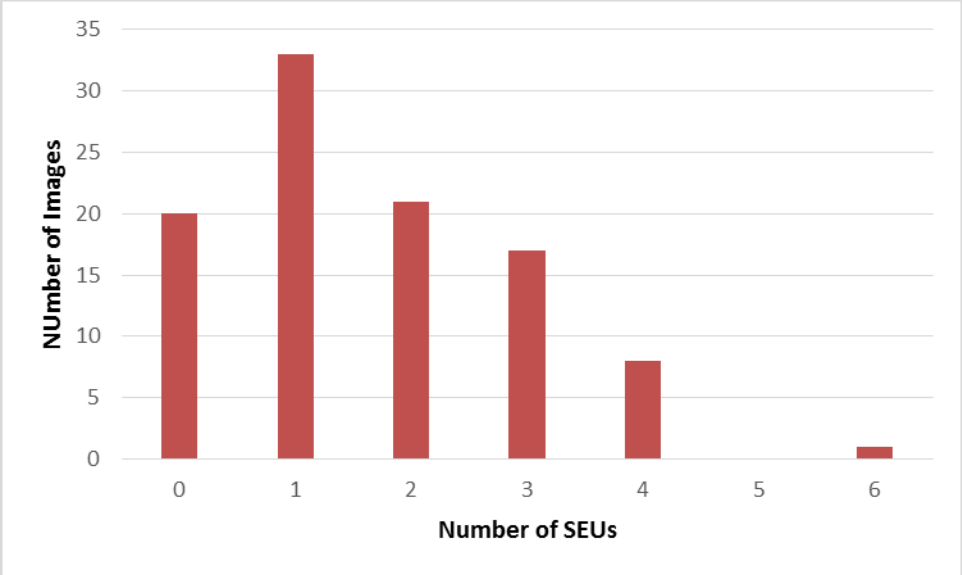

Figure 5.8. Distribution of # of SEUs per image (ISO 1600, t=10s) – Canon 5D MII, 6.26 µm – Peak ~ 1 event/image

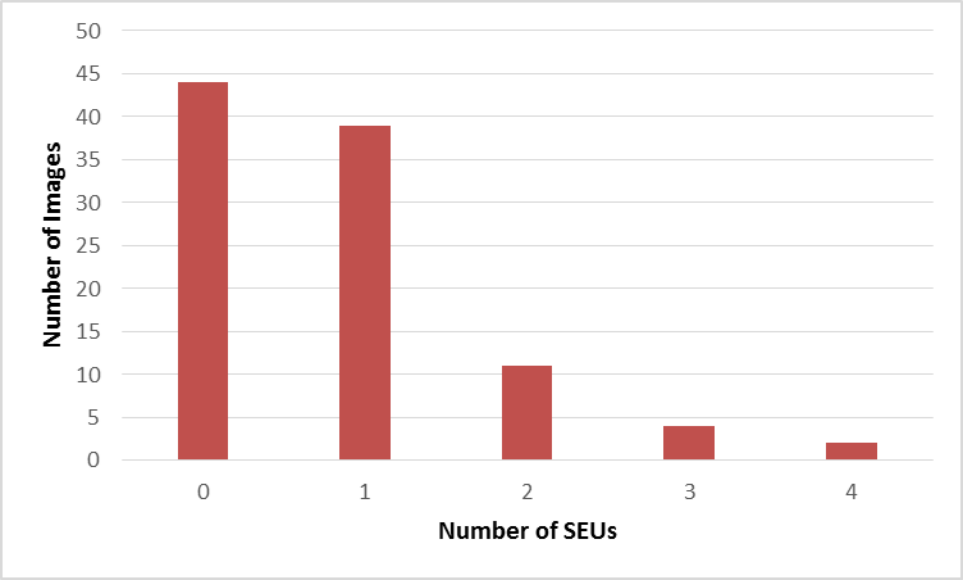

Figure 5.9. Distribution of # of SEUs per image (ISO 1600, t=3.2s) – Canon 5D MII, 6.26 µm – Peak ~ < 1 event/image

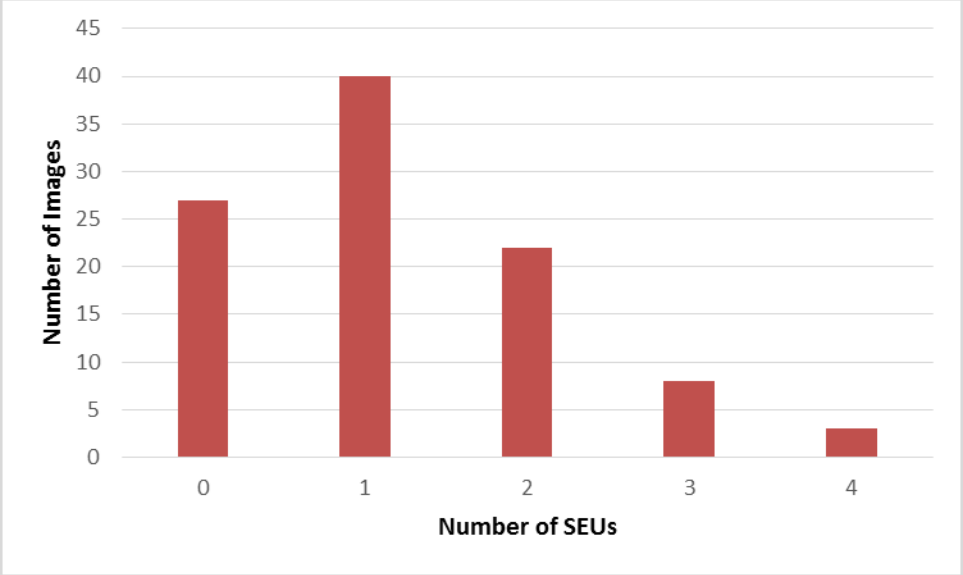

Figure 5.10. Distribution of # of SEUs per image (ISO 1600, t=1s) – Canon 5D MII, 6.26 µm – Peak ~ 1 event/image

These results indicate, as is expected, that the defect rate increases as the exposure time increases. For radiation type events, a common assumption is that their number follows a Poisson process [40]. Given that SEUs occur randomly, the Poisson

distribution is suitable for such cases as it expresses the probability of a given number of events occurring in a fixed interval window if these events occur with a known average rate and independently of the previous event. This type of distribution is commonly used in radiation event rates. The Poisson distribution is shown in Equation 5.1, where λ is the event rate (per second), λt is the expected value of the number of events occurring in t seconds, and k is the number of events in an imager.

$$P(k, \lambda, \mathrm{t}) = \frac{(\lambda \mathrm{t})^k e^{-\lambda \mathrm{t}}}{k!} \tag{5.1}$$

For each value of t, we estimated the expected value λt. Figure 5.11 plots λt for ISO 6400 and ISO 1600 over a range of exposure lengths t. Note that in this plot the exposure time is in a log scale. Figure 5.11 suggests that SEU defect rates increase with ISO. However, this increase is not constant over exposure times. It is clear that for larger exposure times, the increase is greater (with a slope of approximately 0.069 SEUs/second), while for smaller exposure times the difference is much smaller. Also, note that there is a drop in the defect count below the 3.2s exposures for both ISO 1600 and ISO 6400. From the images analyzed, there is a definite reduction in noise from 1s to 3.2s. This sudden change in noise levels implies a sudden change in the SEU events. Though not fully understood at this point, it should be noted that the camera performs some level of background dark frame subtraction around the 1s exposure point. For exposures greater than about 1 s, the camera sequentially takes a dark field image in addition to the exposed image, which is then subtracted from the original data to reduce noise in the image before presenting the data. This subtraction threshold possibly produces the sudden change in the curves at this point as it modifies the background noise level suddenly.

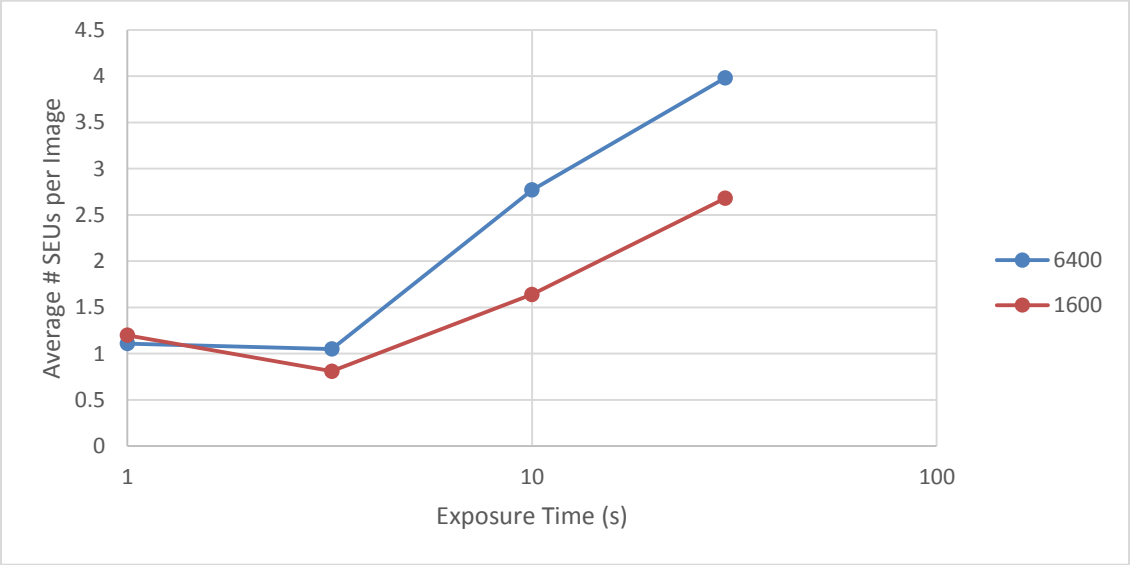

Figure 5.11. Average number of SEUs per image vs exposure time for 1600 and 6400 ISO settings (log scale)

To further illustrate the effects of ISO on the defect rate, we plotted the averages λt for ISO 100, 200, 400, 800, 1600, 3200 and 6400 as shown in Figure 5.12 for two different imagers. For each ISO, the exposure time was fixed at t=30s. It is clear that the defect rate increases with ISO. For camera A from ISO 800 onwards the defect rate grows linearly with ISO at 0.26×10^{-3} SEU/ISO. At ISO 400 and lower ISOs the rate suddenly falls showing the gain is too small for many SEU's to be seen above the noise Threshold. An interesting point is that the ISO400 images do not show the streaks that are seen at higher ISOs. This suggests that there may be several different causes of SEUs (i.e., different cosmic ray particles types creating different effects). The streaks are lower energy events, thus producing many less electrons, and are therefore not evident in the lower ISOs. Camera B shows a similar behavior, but the linear region starts at ISO400, and the slope is 1.01×10^{-3} SEU/ISO or 4.3x steeper. This may reflect the camera differences, of larger sensor area and smaller pixels (see Table 5.1). This plot scales the rate to the Camera A sensor size.

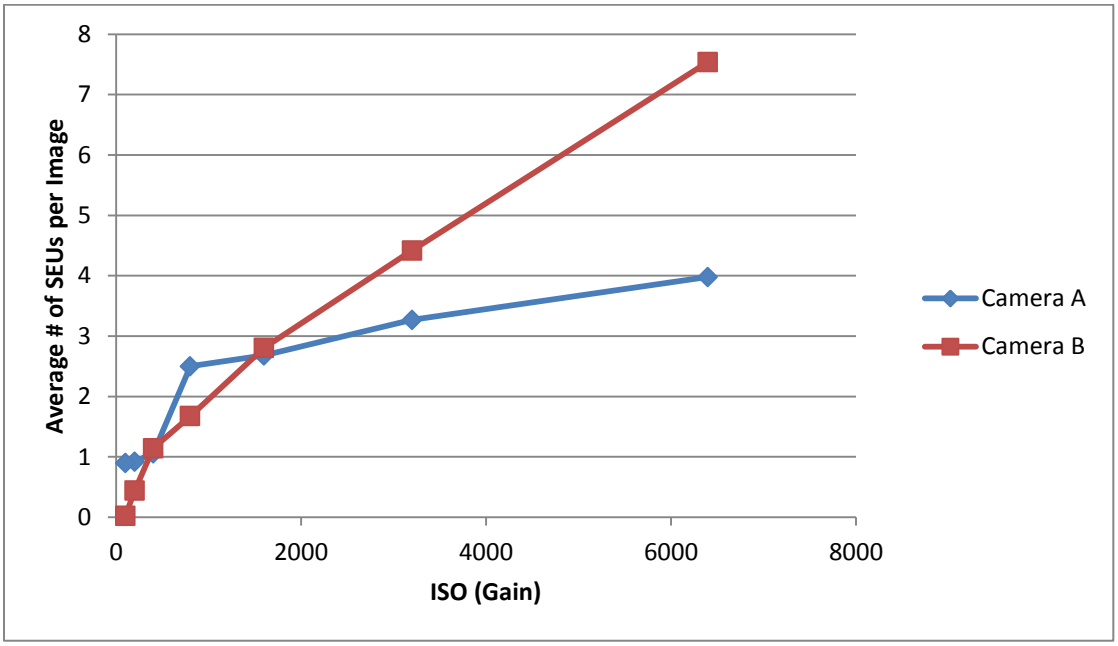

Figure 5.12. Average number of SEUs per image vs ISO (for a 30s exposure) for 2 cameras scaled to camera A (36x24mm)

One question that we have not answered yet is what the exact cause is for SEUs in digital imagers. Traditional studies point towards neutron particles being the primary cause [41]. Literature discussion suggests that muons (generated by secondary cosmic particles) are the likely source of these streak-like errors [42]. In traditional IC defect analysis, SEUs are commonly thought of as single points rather than a spread of charge. This research shows that spread type defects in the form of SEU clusters or streaks are clearly possibly in digital imagers and potentially common ICs. Though a definite answer is yet to be determined, the trend in Figure 5.12 suggests that a combination of neutrons and muons causes these SEU defects. Firstly, at low ISOs we see that almost all defects are single spots and not the clustered kind. Additionally, the number of clusters increases as the ISO increases. Other researchers have identified streaks in imagers as being caused by cosmic ray generated muons, which are lower energy events than the cosmic ray neutrons [43]. This leads us to believe that muons are the probable cause of streak defects, while neutrons more likely generate single pixel defects (similar to what is seen in digital IC circuits).

Table 5.1. SEU Defect Rates for 3 APS Digital Imagers (t=10s, ISO 1600)

Camera	λt	λt/cm^2	Sensor Size (mm × mm)	Pixel (μm)
A	1.640	0.189	36.0 × 24.0	6.26
B	0.481	0.145	22.3 × 14.9	4.30
C	0.654	0.190	22.7 × 15.1	7.38

To confirm that similar behavior is observed across different imagers, we have performed tests on two additional cameras at ISO 1600 with a *t*=10s exposure time as shown in Table 5.1 (A is the camera used in the previous sections). All the imagers in this table have APS sensors and the experiments were conducted and analyzed using the same methodology. For all three cameras, the average number of defects *λt* was extracted. However, each camera has a different sensor size which means that the *λt* values cannot be directly compared, but have to be scaled by the sensor area of the camera.

The results of Table 5.1 tell us some important points. Firstly, SEUs are not limited to one imager but are observable in multiple imagers, making the research repeatable. Secondly, the rates of SEU defects for each camera are fairly consistent. Cameras A and C have higher rates that are quite close to each other. It should be noted that Camera B has smaller pixels (4 μm compared to 7) which may indicate that the pixel size has an impact on the SEU rate. Though Camera B has a smaller rate at ISO 1600, at higher ISOs it is observed that the rate can increase to greater than that of Camera A.

The SEU rate that we have observed for digital imagers, of about 4 SEUs for every 30 seconds, is considerably higher than what was previously reported for ordinary ICs and our expectations when running initial experiments. Permanent hot pixels for the same imager have a rate of about 1 every 12.6 days by our previous measurements [44], so SEUs are 145,000 times more common. By comparison, for ordinary ICs the literature indicates that SEUs are about 100 times more common than permanent faults. This much higher rate in digital imagers is most likely the result of the greater sensitivity of pixels to injected charges. However, as Figure 5.12 suggests, it may also be that imager SEU's are detecting other cosmic ray events, such as muons, that do not affect other digital circuits.

Table 5.1 also suggests the important area that we do not yet have enough data to explore. In the case of hot pixels we saw a strong power law relationship between the pixel size and the hot pixel development rate. We need to see how the hot pixel rate versus SEU rate changes as a function of pixel size.

5.4. SEU Charge Analysis

An ongoing goal of this research is to analyze the charge generated by the SEU events. The intent is to extract the charge of the SEU event by looking at the RAW pixel values. To begin estimating the charge of an SEU event, an assumption that is made is that it takes about 40K electrons to reach saturation for a 7 µm CMOS pixel at ISO 100, a typical value listed in the literature. Note the actual value of 40K is not relevant as the calculations that proceed are relative to this value since it is taken as a baseline. The electron count needed for saturation halves as the ISO doubles. Additionally as the area goes down by a factor of 2, the needed number of electrons also decreases by a factor of 2. Using this analysis, the charge of the SEU events can be derived from the extracted data in the experiments.

Figure 5.13 displays the normalized SEU rate for three imagers as a function of the associated charge. We denote this normalized rate by $\lambda(c)$ and define it as the expected number of SEUs with charge c per year, per mm² of the IC. We can see that the curves for the two cameras with the smaller pixel sizes are very close while the curve for camera 2 deviates. It should be noted that camera 2 is an imager with a larger pixel size which suggests that the size of the pixel may have an impact on the overall SEU rate. As mentioned earlier, this area of SEU research is in the early stages of analysis and further analysis and study is required in this area.

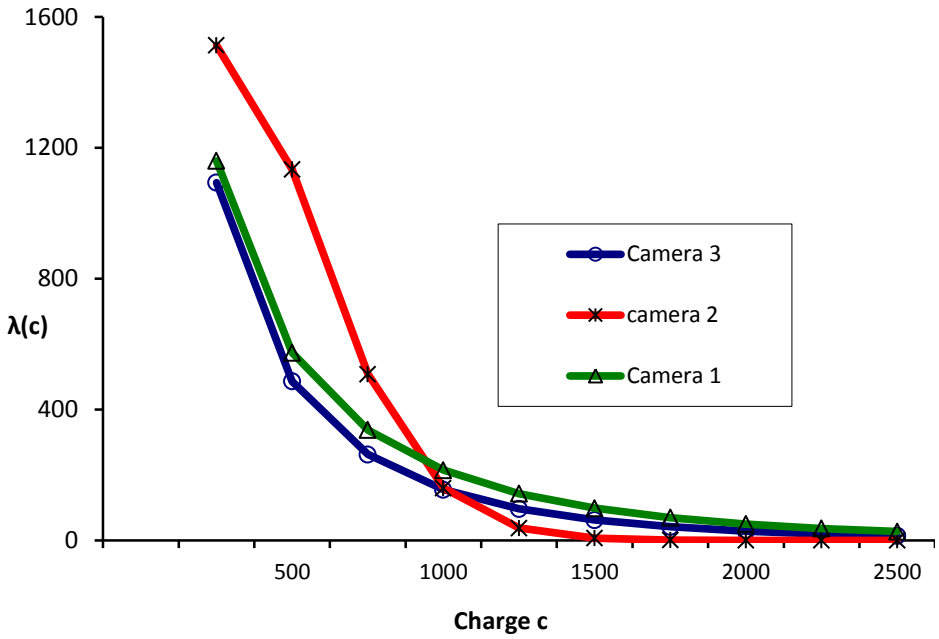

Figure 5.13. Normalized SEU rate λ(c) as a function of the charge

5.5. Summary

This chapter has demonstrated that SEUs occur much more often in digital imagers than in regular ICs, and obviously, more often than permanent hot pixels. As SEUs are easily detectable in digital imagers, further study on the rate as a function of the amplitude (the amount of charge injected by the particle hit) is needed. Such a study can prove to be useful for SEUs in regular ICs as well. Further research will determine how the ratio between the SEU rate and hot pixel rate varies with the imager parameters.

The SEU rate that we have observed for digital imagers, of about 4 SEUs for every 30 seconds, is considerably higher than has been reported for ordinary ICs. Permanent hot pixels for the same imager have a rate of about 1 every 12.6 days, so SEUs are 145,000 times more common. By comparison, for ordinary ICs the literature indicates that SEUs are about 100 times more common than permanent faults. This

much higher rate in digital imagers is most likely the result of the much higher sensitivity of pixels to injected charges. However, as this research suggests, it may also be that imager SEUs are detecting other cosmic ray events, such as muons, that do not affect other digital circuits.

Chapter 6.

Conclusion

6.1. Overview

The previous chapters have explored digital imager pixels in great detail. Emphasis was put on CMOS type pixels due to major trends in today's digital imager market and the limit application use-case for CCD sensors. In Chapter 2, this thesis has demonstrated the overall behaviour of imager pixels and their integration into a larger digital camera system. From low level CMOS design and pixel response curves, the sensor's interaction with incoming light in normal operations was clearly demonstrated. Additionally, the overall benefits of digital photography in contrast to film based cameras were clear. Trends have shown that the traditional film based cameras have been more-or-less phased out and the market is dominated with digital imagers. Moreover, the emergence of cellphone imagers and smaller pixel designs has started to shift the market once more. The average consumer prefers small and more compact digital imagers that can be found in cellphones and other portable devices. There is an evident push in the industry to reduce pixel sizes and increase overall sensor density. With such trends there are definite trade-offs.

The main focus of this thesis is the issue of defects in digital imagers. As mentioned in earlier chapters, the concept of defects and faults in an imager can be quite vast. From hardware to software, many areas of the system are susceptible to defects and eventual infield faults. This research focuses on pixel defects that cause

incorrect pixel output values during camera operation. Two classes of defects were explored – permanent defects that develop infield and temporal or soft defects.

As discussed in Chapter 3, hot pixels are the main type of permanent defect and were the focus of this research for this class of defects. Generally believed to be caused by cosmic rays, hot pixels are damaged pixels that do not follow the standard pixel response. Instead, we have shown that in the presence of a dark field, these pixels will output values. Various types of pixels were shown such as stuck, partially stuck and standard hot pixels. The main goal of this research is to analyze and understand the growth rate of these hot pixel defects. It has been shown that hot pixel defects are caused in field and grow over time indicating that an imager gains more defects as it gets older. This thesis has outlined an empirical model that predicts the hot pixel growth rate based on ISO and pixel size. Focusing on the pixel size parameter, it is clear that as the size of pixels decrease, the defect rate increases. This is a concern as the industry is moving towards smaller pixels in order to reach higher density values – i.e. more megapixels on the same sensor size. Though an advantage from a marketing perspective, these small pixels are a concern as manufacturers do not fully understand the implications from a defect growth concept. Specifically as the market has moved to smaller pixels in the 2 to 1 µm range, the defect growth has accelerated. This research has studied a number of cellphone and DSLR imagers and empirical data has been captured to validate the theory of accelerated defect growth at pixel sizes less than 2 µm. Limitations at the time of this thesis (circa 2016) such as limited RAW support from certain cellphones such as iOS variants proved to be a challenge when focusing on this range of pixels. An updated empirical model has been presented with the enhanced cellphone data as seen in Equation 3.10. The updated model is still within the error bounds of the original model and generally projects the same trends. This model indicates that if the pixel size is shrunk by a factor of 2, then the defect rate will increase by 8.9 times. Similarly, if the ISO is doubled, the defect rate will increase the power of 0.522. The Pearson's r coefficient for this fit is r=0.91, indicating a strong fit. As shown in Figure 3.13 this research has significantly increased coverage at smaller pixel sizes and larger ISO values. The updated growth model is still within the original error bounds with slight changes to the fit parameters.

Hot pixel research has led us to look into SEUs in digital imagers, an area that has not been explored extensively in literature in the past. In literature, soft defects are defined as defects that are temporary and show transient behaviour. They only last for a short amount of time and their effects are not permanent to the circuit itself. Most literature has focused on soft defects in digital ICs – mainly microprocessors and circuits of the like. However, not a lot, if not any discussion has been made on the effects and occurrence of soft defects in digital imagers. A digital sensor is a mixed digital-analog device and is susceptible to the same defect behaviour that traditional digital ICs experience. This thesis has shown that SEUs definitely occur in digital imagers. An experimental setup was created to automate the data collection from imagers. This enabled a large set of data to be collected in an automated fashion. Additionally, a detection software algorithm was developed to detect SEUs in images and generate SEU rates. The experiments mentioned in thesis have studied SEU behaviour over various ISO and exposure time combinations for different DSLR cameras. It has been shown that the overall SEU rate in digital imagers appears to be higher than traditional ICs. The cause of SEUs is typically considered to be cosmic particles hitting the sensor of the camera. The SEU rate for a given imager is about 4 SEUs every 30 seconds. Permanent hot pixels for the same imager have a rate of about 1 every 12.6 days, so SEUs are 145,000 times more common. Literature indicates that ordinary ICs experience SEUs that are about 100 times more common than permanent faults. The SEU rate in digital imagers is much larger and is possibly an avenue for further insight into hot pixel behaviour and charge analysis. This thesis has discovered streak type defects that are believed to be due to a single event that is spread over a larger pixel area, a concept that has not been explored in traditional IC defect analysis.

6.2. Future Research

This thesis has provided an in-depth analysis of hot pixel growth rates and current trends at lower pixel sizes. However, due to limitations in commercially available cell phones, only a handful of cellphone imagers were used in this research as they were the models that only supported RAW output. As technology improves, this research

should be expanded to cover a broader range of cellphone imagers including iOS and other Android based platforms. Additionally, DSLR manufacturers will also begin pushing pixel sizes to these ranges as well which calls for an interesting comparison of the defect rates between DSLRs and cellphone imagers in this small pixel range. The software tools that have developed for cellphone imagers in this thesis can be used for future data and analysis as pixel sizes shrink.

Another avenue for further expansion is the area of hot pixels in light frame fields. All of the research presented in this paper has looked at hot pixels in dark frame fields. From capture, to detection and analysis, no background illumination was present. To fully model hot pixels, their behaviour in the presence of light is vital. Complications in this area are bound to arise as this type of research is susceptible to much more noise and could possibly lead to non-linear behaviour. However, this model of hot pixels in light is vital for manufacturers to be able to quantify their impact and potentially even correct for them in-field.

The SEU research presented here solely looked at DSLR imagers due to restrictions with technology. DSLR imagers are the only type of cameras that enabled remote shooting such that we could take 100+ consecutive images to detect SEUs. In the future as cellphones become mainstream, they will support remote shooting and other functions that current day DSLRs possess. The SEU analysis needs to be enhanced compare rates between camera types and pixel sizes. Additionally, the area of charge analysis in our SEU research is in its infancy. Further work needs to be performed to understand the charge behaviour created by these transient events and their dependency to pixel size, ISO and exposure time. Furthermore, our initial results showed some anomalies in the charge behaviour between cameras which at this stage have not been explained. Further study in this is needed to fully explain the charge behaviour due to SEUs. Additionally, as cellphone support for RAW increases, the SEU research should be extended to include cellphone imagers.

6.3. Concluding Thoughts

It is clear that as the digital IC industry advances to smaller transistor sizes and higher density designs, this trend directly affects the photography industry as well. Digital cameras are also experiencing constant change in that manufacturers are pushing pixels to smaller and smaller sizes with an increased need for sensitivity. As discussed in this thesis, such a push comes at cost in the inherent defect behaviour of the sensors themselves. Though modern designs have been successful to increase pixel density and reduce the relative size of the pixels themselves, sensor designers have not considered the impact of defect growth rates at smaller technology nodes, especially as pixel sizes begin to move to less than 1 µm.

This thesis has explored in detail the various concerns and problematic trends that are occurring at the smaller micron pixel sizes. It is clear that an accelerated defect growth is taking place and it is vital for camera manufacturers to design against such a rapid defect growth trend. Additionally, it has been shown that temporal defects like SEUs are also more prevalent in digital imagers in comparison to traditional digital ICs. Though it does sound comical, this research suggests that as pixel sizes reach lower values, the defect growth rate approaches infinity. However, this statement is what is currently occurring in digital imagers. We are seeing an accelerated growth trend which is concerning when one begins to think about future implications for next generation imagers. Manufacturers of digital imagers need to consider the quality of imagers as pixel sizes decrease. Such concerns further illustrate the need for greater research and investment in the area of digital imager defect analysis and prevention.

References

[1] PetaPixel, “Photography and Camera Reviews,” April 4 2015; http://petapixel.com/2015/04/09/this-is-what-the-history-of-camera-sales-looks-like-with-smartphones-included.

[2] Wordpress, “Charles Arthur's Wordpress,” Feb. 9 2015; https://theoverspill.wordpress.com/2015/02/09/android-oem-profitability-and-the-most-surprising-number-from-q4s-smartphone-market.

[3] Camera Phone Report, “Reiter’s Camera Phone Report,” May 26 2006; http://www.cameraphonereport.com/2006/05/camera_phones_s.html.

[4] E. A. Amerasekera, F. N. Najm, Failure Mechanisms in Semiconductor Devices 2nd ed., New York, NY: John Wiley & Sons, Inc., 1997.

[5] Reliability in CMOS IC Design: Physical Failure Mechanisms and their Modeling, IN MOSIS Technical Notes, http://www.mosis.org/support/technical-notes.html.

[6] Leung, J. (2011). Measurement and Analysis of Defect Development in Digital Imagers (Master’s thesis, Simon Fraser University, Burnaby, Canada). Retrieved from http://www.lib.sfu.ca.

[7] G. Chapman, R. Thomas, I. Koren, and Z. Koren, “Relating digital imager defect rates to pixel size, sensor area and ISO,” Proc. of the 2012 IEEE Intern. Symposium on Defect and Fault Tolerance in VLSI Systems, 164-169, Austin, TX, Oct. 2012.

[8] J. Dudas, L. M. Wu, C. Jung, G. H. Chapman, Z. Koren, I. Koren,“Identification of in-field defect development in digital image sensors”, in Proc. Electronic Imaging, Digital Photography II, V6502, 6502Y1-0Y12, San Jose, Jan. 2007.

[9] J. Leung, G.H. Chapman, I. Koren, and Z. Koren, “Statistical Identification and Analysis of Defect Development in Digital Imagers,” Proc. SPIE Electronic Imaging, Digital Photography V, v7250, 742903-1 – 03-12, San Jose, Jan 2009.

[10] A.J.P. Theuwissen, “Influence of terrestrial cosmic rays on the reliability of CCD image sensors. Part 1: experiments at room temperature,” IEEE Transactions on Electron Devices, Vol. 54 (12), 3260-6, 2007.

[11] A.J.P. Theuwissen, “Influence of terrestrial cosmic rays on the reliability of CCD image sensors. Part 2: experiments at elevated temperature,” IEEE Transactions on Electron Devices, Vol. 55 (9), 2324-8, 2008.

[12] J. Leung, G. Chapman, I. Koren, and Z. Koren, “Automatic Detection of In-field Defect Growth in Image Sensors,” Proc. of the 2008 IEEE Intern. Symposium on Defect and Fault Tolerance in VLSI Systems, 220-228, Boston, MA, Oct. 2008.

[13] J. Leung, G. H. Chapman, I. Koren, Z. Koren, “Tradeoffs in imager design with respect to pixel defect rates,” Proc. of the 2010 Intern. Symposium on Defect and Fault Tolerance in VLSI, 231-239., Kyoto, Japan, Oct 2010.

[14] G.H. Chapman, R. Thomas, I. Koren, and Z. Koren, “Empirical formula for rates of hot pixel defects based on pixel size, sensor area and ISO”, Proc. Electronic Imaging, Sensors, Cameras, and Systems for Industrial/Scientific Applications XIII, v8659, 86590C-1-C-11 San Francisco, Jan. 2013.

[15] R. Heald, 'How Cosmic Rays Cause Computer Downtime', IEEE Rel. Soc. SCV Meeting, 2005.

[16] Wipac.wisc.edu, 'Deco'. [Online]. Available: http://wipac.wisc.edu/deco. [Accessed: 15- May- 2015].

[17] Wikipedia, “PN-Junction Diodes,” Aug. 1 2012; https://en.wikibooks.org/wiki/Analogue_Electronics/pn_Junctions.

[18] J. Nakamura, "Basics of image sensors," in Image Sensors and Signal Processing for Digital Still Cameras J. Nakamura, Ed. Boca Raton, FL: Taylor & Francis Group, 2006, pp. 55-59.

[19] Openwetware, “Diodes,” Sept. 10 2006; http://openwetware.org/wiki/20.309:DiodePrimer.

[20] H. Lin, C.H Lai and Y. C. Ling (2004). "A four transistor CMOS active pixel sensor with high dynamic range operation". IEEE Advanced System Integrated Circuits: 124–127.

[21 L. Blanquart, "Global shutter pixel circuit with transistor sharing for CMOS image sensors," U.S. Patent: 250/208.1, issued date April 30, 2009.

[22] La Haye, M. (2007). Enhancing Sensitivity for Active Pixel Sensor with Fauly Tolerance and Demosaicing (Master's thesis, Simon Fraser University, Burnaby, Canada). Retrieved from http://www.lib.sfu.ca.

[23] Betanews, "Image Sensor Unit Shipments," Nov. 7 2011; http://betanews.com/2011/11/07/kodak-sells-off-its-ccd-image-sensor-business-to-private-equity-firm.

[24] Nakamura, Junichi (2005). Image Sensors and Signal Processing for Digital Still Cameras. CRC. ISBN 0-8493-3545-0.

[25] A.J.P. Theuwissen, "Influence of terrestrial cosmic rays on the reliability of CCD image sensors. Part 1: experiments at room temperature," IEEE Transactions on Electron Devices, Vol. 54 (12), 3260-6, 2007.

[26] A.J.P. Theuwissen, "Influence of terrestrial cosmic rays on the reliability of CCD image sensors. Part 2: experiments at elevated temperature," IEEE Transactions on Electron Devices, Vol. 55 (9), 2324-8, 2008.

[27] J. Dudas, L.M. Wu, C. Jung, G.H. Chapman, Z. Koren, and I. Koren, "Identification of in-field defect development in digital image sensors," Proc. Electronic Imaging, Digital Photography III, v6502, 65020Y1-0Y12, San Jose, Jan 2007.

[28] J. Leung, J. Dudas, G. H. Chapman, I. Koren, Z. Koren, "Quantitative Analysis of In-Field Defects in Image Sensor Arrays," Proc. 2007 Intern. Sym on Defect and Fault Tolerance in VLSI, 526-534, Rome, Italy, Sept 2007.

[29] G. Chapman, R. Thomas, I. Koren, and Z. Koren, "Improved image accuracy in Hot Pixel degraded digital cameras," Proc. of the 2013 IEEE Intern. Symposium on Defect and Fault Tolerance in VLSI Systems, 172-177, New York, NY, Oct. 2013.

[30] G. H. Chapman, R. Thomas, Z. Koren, I. Koren, "Correcting High Density Hot Pixel Defects in Digital Imagers", in Proc. Electronic Imaging, Digital Photography II, V9022, 90220G, San Jose, March 2014.

[31] Draper, N. (1998). Applied Regression Analysis, 3rd Edition. New York, NY: Wiley.

[32] G. H. Chapman, J. Leung, R. Thomas, A. Namburete, Z. Koren, I. Koren, “Projecting the rate of in-field pixel defects based on pixel size, sensor area, and ISO”, in Proc. Electronic Imaging, Digital Photography II, V8298, 82980E, San Jose, Feb 2012.

[33] Oakdale Engineering, “DataFit,” http://www.oakdaleengr.com.

[34] G.H. Chapman, R. Thomas, I. Koren, and Z. Koren, “Empirical formula for rates of hot pixel defects based on pixel size, sensor area and ISO”, Proc. Electronic Imaging, Sensors, Cameras, and Systems for Industrial/Scientific Applications XIII, v8659, 86590C-1-C-11 San Francisco, Jan. 2013.

[35] J. Leung, G. H. Chapman, I. Koren, Z. Koren, “Tradeoffs in imager design with respect to pixel defect rates,” Proc. of the 2010 Intern. Symposium on Defect and Fault Tolerance in VLSI, 231-239., Kyoto, Japan, Oct 2010.

[36] R. Heald, 'How Cosmic Rays Cause Computer Downtime', IEEE Rel. Soc. SCV Meeting, 2005.

[37] Wipac.wisc.edu, 'Deco'. [Online]. Available: http://wipac.wisc.edu/deco. [Accessed: 15- May- 2015].

[38] Kurzweilai.net, 'How to turn your Android phone into a cosmic ray detector', 2014. [Online]. Available: http://www.kurzweilai.net/how-to-turn-your-android-phone-into-a-cosmic-ray-detector. [Accessed: 15- May- 2015].

[39] J. Leung, G. H. Chapman, I. Koren, Z. Koren, “Tradeoffs in imager design with respect to pixel defect rates,” Proc. of the 2010 Intern. Symposium on Defect and Fault Tolerance in VLSI, 231-239., Kyoto, Japan, Oct 2010.

[40] Frank A. Haight (1967). Handbook of the Poisson Distribution. New York: John Wiley & Sons.

[41] R. Heald, 'How Cosmic Rays Cause Computer Downtime', IEEE Rel. Soc. SCV Meeting, 2005.

[42] Wipac.wisc.edu, 'Deco'. [Online]. Available: http://wipac.wisc.edu/deco. [Accessed: 15- May- 2015].

[43] Kurzweilai.net, 'How to turn your Android phone into a cosmic ray detector', 2014. [Online]. Available: http://www.kurzweilai.net/how-to-turn-your-android-phone-into-a-cosmic-ray-detector. [Accessed: 15- May- 2015].

[44] J. Leung, G.H. Chapman, Y.H. Choi, R. Thomson, I. Koren, and Z. Koren, “Tradeoffs in imager design parameters for sensor reliability,” Proc., Electronic Imaging, Sensors, Cameras, and Systems for Industrial/Scientific Applications XI, v 7875, 78750I1-0I12, San Jose, Jan. 2011.

Appendix A.

List of APS Imagers

- Canon EOS10D
- Canon EOS5DMarkII
- Canon EOS300D
- Canon EOS450D
- Canon EOS350D
- Canon EOS450D
- Canon EOS20D
- Canon EOS350D
- Canon EOS30D
- Nikon D2x
- Canon EOS550D (T2i MS)
- Pentax K7
- Canon EOS550D (T2i AC)
- Canon T1i (MS)
- Canon T3i (J)
- Canon T5i (RT)
- Nexus 5 Sony IMX175
- Oneplus One a0001
- Nexus P6
- Samsung S6